

A 1.5Ma Marine Record of Volcanic Activity and Associated Landslides Offshore Martinique (Lesser Antilles): Sites U1397 and U1399 of IODP 340 Expedition

Benoît Villemant, Anne Le Friant, Benoît Caron, Giulia del Manzo, Sara Lafuerza, Laurent Emmanuel, Osamu Ishizuka, Hervé Guyard, Nathalie Labourdette, Agnès Michel, et al.

▶ **To cite this version:**

Benoît Villemant, Anne Le Friant, Benoît Caron, Giulia del Manzo, Sara Lafuerza, et al.. A 1.5Ma Marine Record of Volcanic Activity and Associated Landslides Offshore Martinique (Lesser Antilles): Sites U1397 and U1399 of IODP 340 Expedition. Frontiers in Earth Science, 2022, 10, pp.767485. 10.3389/feart.2022.767485 . hal-03619699

HAL Id: hal-03619699
https://hal.science/hal-03619699

Submitted on 25 Mar 2022

HAL is a multi-disciplinary open access archive for the deposit and dissemination of scientific research documents, whether they are published or not. The documents may come from teaching and research institutions in France or abroad, or from public or private research centers.

L'archive ouverte pluridisciplinaire **HAL**, est destinée au dépôt et à la diffusion de documents scientifiques de niveau recherche, publiés ou non, émanant des établissements d'enseignement et de recherche français ou étrangers, des laboratoires publics ou privés.

frontiers in Earth Science

ORIGINAL RESEARCH
published: 24 March 2022
doi: 10.3389/feart.2022.767485

A 1.5 Ma Marine Record of Volcanic Activity and Associated Landslides Offshore Martinique (Lesser Antilles): Sites U1397 and U1399 of IODP 340 Expedition

Benoît Villemant[1], Anne Le Friant[2], Benoît Caron[1], Giulia Del Manzo[2], Sara Lafuerza[1], Laurent Emmanuel[1], Osamu Ishizuka[3], Hervé Guyard[2], Nathalie Labourdette[1], Agnès Michel[2†] and Samia Hidalgo[2]*

[1]Institut des Sciences de la Terre Paris (ISTEP), Sorbonne Université, Paris, France, [2]Institut de Physique du Globe de Paris (IPGP), Paris, France, [3]Geological Survey of Japan, National Institute of Advanced Industrial Science and Technology, AIST, Tsukuba, Japan

OPEN ACCESS

Edited by:
Michel Pichavant, CNRS Orléans, France

Reviewed by:
Sebastian Watt, University of Birmingham, United Kingdom
Armin Freundt, Helmholtz Association of German Research Centres (HZ), Germany

***Correspondence:**
Benoît Villemant
benoit.villemant@sorbonne-universite.fr

†AM deceased

Specialty section:
This article was submitted to Volcanology, a section of the journal Frontiers in Earth Science

Received: *30 August 2021*
Accepted: *18 February 2022*
Published: *24 March 2022*

Citation:
Villemant B, Le Friant A, Caron B, Del Manzo G, Lafuerza S, Emmanuel L, Ishizuka O, Guyard H, Labourdette N, Michel A and Hidalgo S (2022) A 1.5 Ma Marine Record of Volcanic Activity and Associated Landslides Offshore Martinique (Lesser Antilles): Sites U1397 and U1399 of IODP 340 Expedition. Front. Earth Sci. 10:767485. doi: 10.3389/feart.2022.767485

The products of eruptive and mass-wasting processes that built island arc volcanoes are better preserved in marine deposits than on land. Holes U1397A and U1399A drilled during IODP Expedition 340 provide a 1.5 Ma record of the volcanic history of Martinique. ^{14}C dating and $\delta^{18}O$ patterns are used to reconstitute the chronostratigraphy of tephra, volcaniclastic turbidites, and mass-wasting events (traced by debris avalanches, debrites, and duplication and deformation of pre-existing sediments), leading to a new volcanic history of Montagne Pelée and Pitons du Carbet volcanoes. The top 50 m of core U1397A provides a continuous high-resolution sedimentation record over the last ~130 ka. The sedimentation record deeper than 50 m in core U1397A and in the whole core U1399A is discontinuous because of the numerous sliding and deformation events triggered by debris avalanches related to flank collapses. Three successive activity periods are identified since ~190 ka: the "Old Pelée" until 50 ka, the "Grand Rivière" (50–20 ka), and the "Recent Pelée" (20 ka—present day). The first two periods have the highest volcanic deposition rates offshore but very little outcrop on land. The whole magmatic activity of Mt Pelée comprises silicic andesites, but mafic andesites were also emitted during the whole "Grand Rivière." At ~115 ka, a major flank collapse ("Le Prêcheur") produced a debris avalanche and submarine landslide that affected sea floor sediments by erosion and deformation up to ~70 km from the shore. The Pitons du Carbet volcano was active from 1.2 Ma to 260 ka with numerous large flank collapses at a mean rate of 1 event every 100 ka. The average deposition rate of tephra fall offshore is much less than that at Mt Pelée. Our data show that correlations between the timing of large landslides or emission of mafic magmas and rapid sea level rise or lowstands suggested by previous studies are not systematic. The reconstituted chronostratigraphy of cores U1397A and U1399A provides the framework necessary for further studies of the magma petrology and production rates and timing of the mechanisms triggering flank collapses and related submarine landslides of Mt Pelée and Pitons du Carbet.

Keywords: *Chronostratigraphy*, volcanic tephra, flank collapse, submarine landslides, Caribbean, Mt Pelée volcano, Martinique (FWI: French West Indies), IODP (integrated ocean drilling program) expedition 340

1 INTRODUCTION

Reconstitution of the history of volcanoes of the Lesser Antilles Arc using on-land data is difficult because of the scarcity of outcrops due to 1) the tropical climate that favors the erosion of volcanic deposits and development of a dense vegetation cover and 2) the specific characters of the andesitic volcanic activity: low eruption rates (some eruptions per ka), recurrence of explosive and destructive phases, recurrence of dome-forming eruptions, and scarcity of lava flows that create highly unstable deposits, easily destroyed by flank collapses. In small island environments, the history of the volcanic activity is generally better preserved in the submarine deposits close to the volcano than on-land. In addition, the ^{14}C and ^{18}O records on foraminifera allow construction of a precise chronostratigraphy of the hemipelagic sedimentation and volcanic tephra and debris avalanche deposits intercalated in the marine sedimentary sequence.

Following the approaches of Keller et al. (1978), Carey and Sigurdsson (1980), Paterne et al. (1986), Reid et al. (1996), and Carey (1999), the IODP 340 expedition on the R/V JOIDES Resolution drilled and cored marine sediments at nine sites located off Montserrat and Martinique islands. The objectives were 1) to study deposits related to volcano flank collapses and 2) document the long-term eruptive history of volcanoes. Previous studies from the Lesser Antilles have identified distinctions of two types of offshore deposits related to flank collapse, based on surface morphology, geophysical data, and core sampling (see, for example, Deplus et al., 2001; Watt et al., 2012; Le Friant et al., 2015): debris avalanche deposits (DADs), that are primary deposits of volcano flank collapse, and submarine landslide deposits (SLDs) that are deformed to remobilized seafloor sediments by secondary failures initiated by the DAD. The timing and emplacement processes of landslide deposits inferred from the IODP 340 expedition and previous studies are summarized in the studies by Le Friant et al. (2013), Le Friant et al. (2015), and Le Friant et al. (2020). A series of articles report the eruptive history of Montserrat inferred from the IODP 340 expedition (Jutzeler et al., 2014; Wall-Palmer et al., 2014; Coussens et al., 2016a; Coussens et al., 2016b; Fraass et al., 2017; Jutzeler et al., 2017). Five coring sites (U1397 to U1401) were chosen on the Caribbean western flank of Martinique. One site U1397 was dedicated to sediment chronostratigraphy, and the other sites were dedicated to investigate the SLDs generated by flank collapses of Mt Pelée, the most recent volcano north of Martinique (Lafuerza et al., 2014; Hornbach et al., 2015; Le Friant et al., 2015; Brunet et al., 2016; Brunet et al., 2017; Llopart et al., 2018; Knappe et al., 2020; Le Friant et al., 2020; Mencaroni et al., 2020), combining description of the types of cored sediments (composition, deformation, distribution, and physical properties), high-resolution seismic reflection data, and physical modeling. Only the short (~15 m) core U1401A has been investigated for tephrostratigraphy using a high-resolution ^{14}C and ^{18}O chronology (0 to ~36 ka; Solaro et al., 2020).

This study contributes to the reconstruction of the volcanic history of Martinique using two IODP sites: U1397 close to the coast expected to have the most extensive and better preserved record of the volcanic activity and U1399 at the distal part of the main SLD. ^{14}C and ^{18}O records on Foraminifera (*Globigerinoides ruber* white and pink) provide a precise chronostratigraphy of hemipelagic sediments and document the volcanic activity and flank collapses related to recent activity of Mt Pelée over the last 130 ka. For older periods, despite the disturbance of the sedimentary sequences caused by turbidity currents and landslides driven by gravity or by volcanic activity and flank collapses, it is possible to propose a reconstitution of the history and emplacement mechanisms of these events over ~1.5 Ma as they are recorded in offshore sediments. These new results are compared to on-land data with a special emphasis on the relationship between flank collapses and magmatic evolution of the volcanoes.

2 PREVIOUS WORKS

2.1 Geological Setting and On-Land Volcano History

The Lesser Antilles Arc results from the subduction of the Atlantic oceanic plate beneath the Caribbean Plate, at ~2 cm/yr (Wadge, 1984). North of Dominica, it is divided in two distinct arcs due to the westward migration of the volcanic activity (**Figure 1A**). To the southwest, it is bordered by the 2,900-m deep back-arc Grenada Basin and, to the east, by a large plateau that is cut in the northeast by deep trenches perpendicular to the arc (Feuillet et al., 2002). The volcanic activity started at the north of the arc ~40 Ma ago and progressively migrated to the southwest (Martin-Kaye, 1969; Bouysse et al., 1990). The inner arc includes all active volcanoes of the last 20 Ma. Martinique is located at the junction between the two arcs. The volcanic activity migrated from southeast to northwest of the island since the Early Miocene (Westercamp et al., 1989; Germa et al., 2010, Germa et al., 2011b; Labanieh et al., 2012). Since the Pliocene, the northern part of Martinique was built by the successive activities of Morne Jacob (5.2–1.5 Ma) to the east, Pitons du Carbet (998–322 ka) to the south, Mont Conil (543–127 ka) to the north, and Montagne Pelée (126 ka–present day) located between the last two edifices (Samper et al., 2008; Germa et al., 2011b, Germa et al., 2015; **Figure 2A**). Mt Pelée eruptions have been the subject of numerous studies in volcanology (Lacroix, 1904; Westercamp and Traineau, 1983a; Jaupart and Allègre, 1991; Tanguy, 1994, Villemant and Boudon, 1998; Tanguy, 2004; Carazzo et al., 2012) and petrology (Roobol and Smith, 1976; Bourdier et al., 1985; Gourgaud et al., 1989; Traineau et al., 1989; Fichaut et al., 1989; Villemant et al., 1996; Martel et al., 1998; Pichavant et al., 2002; Annen et al., 2008; Labanieh et al., 2010; Boudon et al., 2013). The recent activity of Mt Pelée from the last eruption in 1929 to about 20 ka is well-established (Westercamp and Traineau, 1983a, Westercamp and Traineau, 1983b; Traineau et al., 1989; Michaud-Dubuy et al., 2019; **Figure 2B**). In addition, the volcanic record is more fragmentary due to the rarity of outcrops and poor dating resolution. Between ~20 and 40 ka, the "Grand Rivière" events are characterized by specific eruptive style and petrology (Bourdier et al., 1985; Boudon et al., 2013). The older activity period (~40–130 ka) called 'Paleo Pelée' is identified

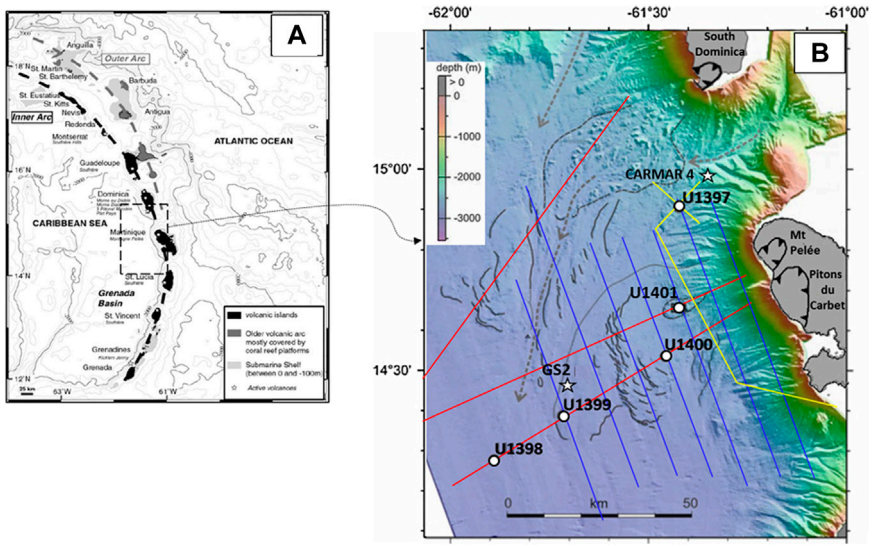


FIGURE 1 | Lesser Antilles Arc, landslide deposits, and IODP 340 coring sites offshore Martinique. **(A)** Two island arcs. The inner arc is the active volcanic arc (modified from Boudon et al. (2007)). **(B)** IODP 340 drilling sites and extent of chaotic units. Submarine topography: swath bathymetry illuminated from the North; gray lines: topographic scarps (DAD3 is the blocky unit above which is located the U1401 site; other scarps correspond to SLDs limits); gray arrows: main deep sea channels. Colored lines are seismic reflection lines used to locate the coring sites (blue: AGUADOMAR cruise, 1999, Red: CARAVAL cruise, 2002, Yellow: GWADASEIS cruise, 2009, Deplus et al., 2001; Le Friant et al., 2003). Drilling sites: open circles: IODP 340 cores; stars: CARMAR-4 (CARAVAL cruise) and GS-2 (Gs7605 cruise; Reid et al., 1996). On-land black scars: flank collapse structures of Martinique (Mt Pelée and Pitons du Carbet) and South Dominica (modified from Boudon et al. (2013)).

in very few outcrops on land. Older volcanic complexes (Mt Conil, Pitons du Carbet, and Morne Jacob) have only been the subject of few petrological or volcanological studies (Westercamp and Traineau, 1983a; Westercamp et al., 1989; Labanieh et al., 2010, Labanieh et al., 2012; Boudon et al., 2013; **Figure 2B**).

Numerous flank collapses have been identified on volcanoes of the Lesser Antilles Arc (Deplus et al., 2001; Le Friant et al., 2002, Le Friant et al., 2003; Boudon et al., 2005, Boudon et al., 2007). Their emplacement and time constraints have been established from offshore drilling data (Le Friant et al., 2013; Wall-Palmer et al., 2014, Le Friant et al., 2015; Brunet et al., 2016; Coussens et al., 2016a; Coussens et al., 2016b; Le Friant et al., 2020). At Mt Pelée, at least three flank collapses have created large horseshoe-shaped structures on the western flank of the volcano and produced DADs on land and offshore (Vincent et al., 1989; Le Friant et al., 2003, Boudon et al., 2005, Boudon et al., 2007, Le Friant et al., 2008; Le Friant et al., 2015; **Figure 2B**). They were identified and first dated by the scars of the collapse structures (Le Friant et al., 2003; Boudon et al., 2005; Germa et al., 2011a; Boudon et al., 2013): "Le Prêcheur" event (between 70 and 127 ka), "Saint Pierre" event (between 30 and 45 ka), and 'Rivière Sèche' event (~10 ka). Recent investigations have questioned this chronology (Le Friant et al., 2015, Brunet et al., 2016; Le Friant et al., 2020; Solaro et al., 2020). At the Pitons du Carbet volcanic complex, a large collapse structure corresponds to one or more flank collapses of the minimum age ~337 ka (Westercamp et al., 1989; Boudon et al., Boudon et al., 2007; Samper et al., 2008, Boudon et al., 2013; **Figure 2B**). Triggering mechanisms of flank collapses and their consequences on volcanic activity have been discussed in a number of articles (see, for example, Quidelleur et al., 2008; Boudon et al., 2013; Le Friant et al., 2015; Coussens et al., 2016b; Brunet et al., 2016; Watt, 2019; Le Friant et al., 2020).

2.2 Submarine Record of the Volcanic History of Martinique

The Endeavour cruise in 1979 gathered a regional collection of piston cores allowing assessments of rates of volcanism and sedimentation, dating of major eruptions, recognition of submarine pyroclastic flow deposits, and establishment of a biostratigraphic framework for the eastern Caribbean (Sigurdsson et al., 1980; Sparks et al., 1980a, Sparks et al., 1980b; Reid et al., 1996). Cruises offshore Montserrat and Martinique islands collected short cores (<10 m) that record the volcanic activity since ~110 ka for Montserrat (Le Friant et al., 2008; Trofimovs et al., 2013) and ~30 ka for Mt Pelée (CARAVAL cruise, Deplus et al., 2001; Boudon et al., 2013). Drillings of the IODP 340 expedition in 2012 considerably widen the studied age ranges (Le Friant et al., 2013). Sites U1394 to U1396 were used to reconstitute the volcanic history of Montserrat over ~1 Ma (Wall-Palmer et al., 2014; Coussens et al., 2016a; Coussens et al., 2016b). Five sites (U1397 to U1401) were drilled offshore Martinique. To better record the volcanic activity, site U1397 is located north-west of the island, close to the coast (~20 km) but far enough from the DADs and SLDs from Mt Pelée and South Dominica (**Figure 1B**). It is located on a topographic high bound by large canyons to be as undisturbed as possible by marine and turbidity currents. It is also close to the piston core CARMAR 4 of the CARAVAL cruise

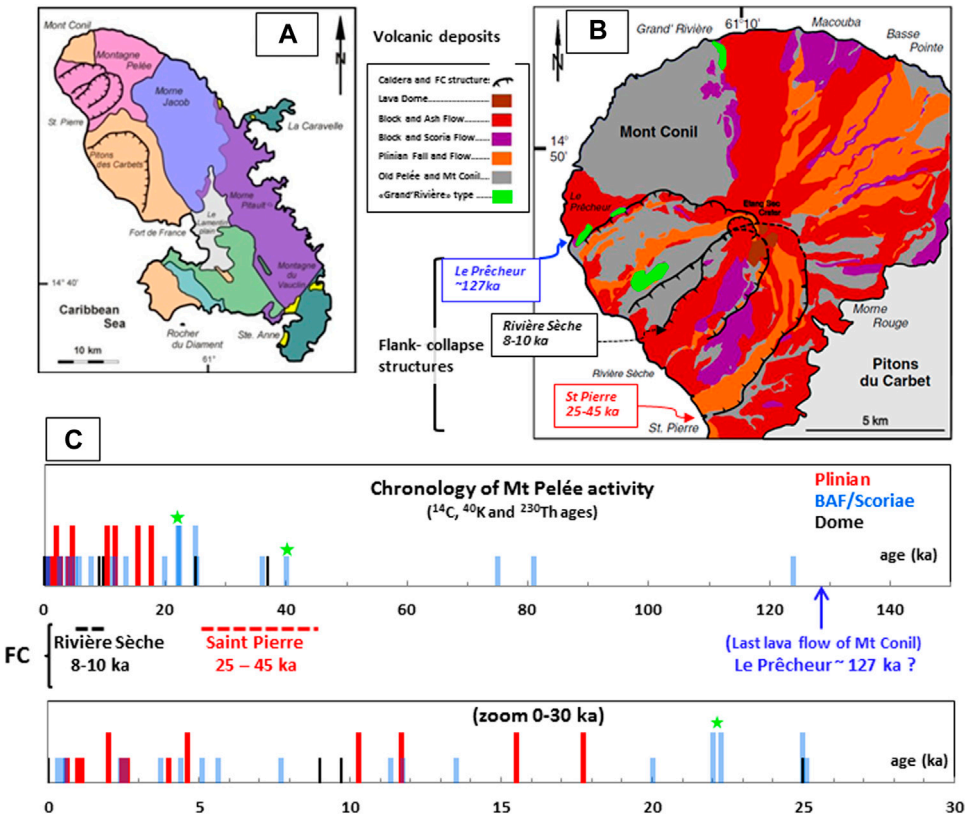


FIGURE 2 | Chronology of the volcanic activity of Martinique. **(A)** Volcanic centers of Martinique (from Germa et al. (2011a)). **(B)** Volcanic deposits and flank collapse structures of Mt Pelée (modified from Le Friant et al., 2003 and Boudon et al., 2013). Flank collapse structures are dated by bracketing with ages of domes grown inside the collapse scarps or cut at collapse structure edges: "Le Prêcheur" (K-Ar[3]); "Rivière sèche" (U-Th[2,5]); and "St Pierre" (K-Ar[3],U-Th[2,5],^{14}C[1]). **(C)** Chronology of the volcanic activity and flank collapse structures of Mt Pelée. Eruptive styles: Dome: lava dome; BAF: block and ash flow; scoriae: scoria fall or flow; Plinian: plinian fall or flow; FC: flank collapses. The height of the bars relates to the relative intensities of the eruptions. Green stars: the two dated "Grand Rivière" events that produced mafic scoriae. Data sources: (1) Westercamp et al., 1989 (^{14}C); (2) Le Friant et al., 2002 (^{14}C-U/Th); (3) Germa et al., 2011a (K-Ar); (4) Michaud-Dubuy (^{14}C), 2019, (5) Villemant et al. (U/Th, unpublished); (6) Ishizuka et al., (^{14}C-K/Ar unpublished); see also **Supplementary Table S3**.

(2002, ~15 km to the NE of site U1397) that collected 7 m of well-bedded sediments with around 50 tephra layers (Boudon et al., 2013). The four other sites are aligned with the flank-collapse structures of Mt Pelée on the seismic line 16 of the CARAVAL cruise (**Figure 1B**). Sites U1399 to U1401 are located on deposits characterized by chaotic facies in seismic reflection (for definition see, for example., Deplus et al., 2001; Lebas et al., 2011; Watt et al., 2012). Site U1398 is the most distant (~80 km) from the shore, beyond the chaotic facies deposits (**Figure 1B**). It mainly contains volcaniclastic turbidites (>70%–95%, Le Friant et al., 2013; Breitkreuz et al., 2021) due to its location on the low slopes inside the Grenada Basin which channeled most turbidity currents from the western flank of the Arc (**Figure 1**). The composition of volcanic clasts, age range, and isotopic and trace element compositions of zircons suggest that the majority of these turbidites originate from Dominica (Breitkreuz et al., 2021). Site U1401, the closest to the shore, penetrates the sediments over 15 m down to the blocky deposit whose drilling was unsuccessful due to its high content in large volcanic blocks, characteristic of a DAD (DAD 3; **Figure 1B**; Le Friant et al., 2015). This DAD is related to the "St Pierre" flank collapse (Brunet et al., 2016) and is older than 36 ka (Solaro et al., 2020).

Compaction of sediments in the upper 200 m of the IODP 340 cores west of Martinique was evaluated from the normalized undrained shear strength measurements on the hemipelagic intervals and correlated with consolidation tests on whole round samples (Lafuerza et al., 2014). Most sediments (except at site U1400) are normally or slightly under-consolidated. High abundance of thick turbidites and coarser tephra explains the pore fluid pressures in slight excess of hydrostatic. However, the upper 120 m of core U1400 and some intervals in the other cores are over-compacted due to vertical erosion and/or deformation. Cores U1399 and U1400 penetrate more than 200 m within sediments typical of SLDs with only few well-bedded sediments interspersed in turbidites and highly deformed

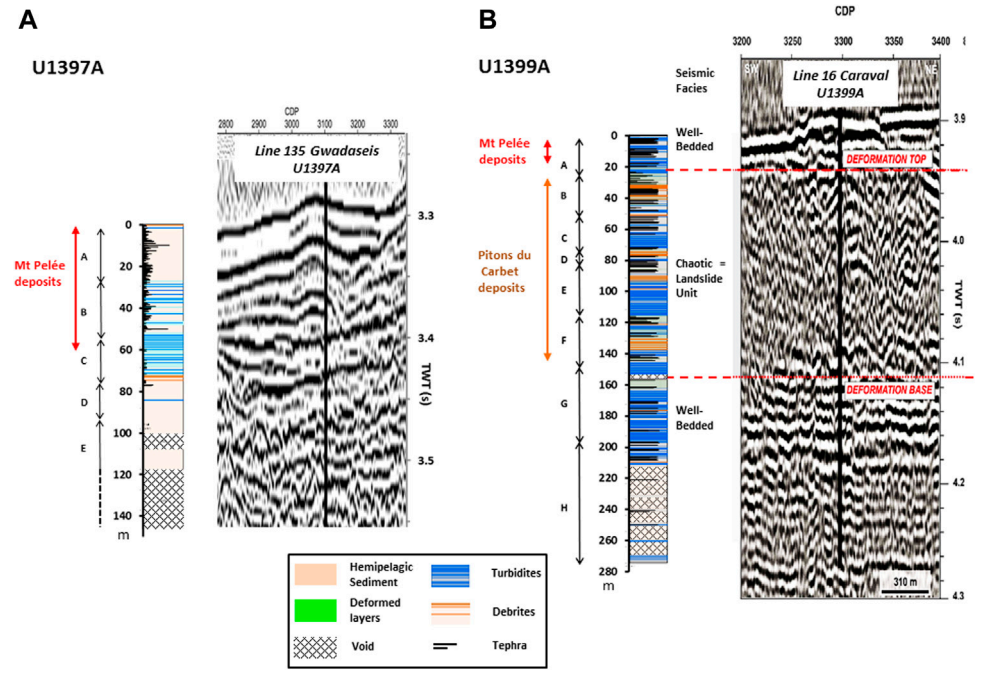


FIGURE 3 | Simplified lithology, deformation figures, and seismic facies of holes 1397A **(A)** and 1399A **(B)**. Seismic data from Brunet et al. (2016) and Le Friant et al. (2015), Le Friant et al. (2020). Depth in core in meter. Letters: lithological units defined on board (Le Friant et al., 2013). The reader is referred to **Supplementary Figure S1** for high-resolution stratigraphic logs on the web version of this article for benefit.

sediments (Le Friant et al., 2013; Lafuerza et al., 2014, Brunet et al., 2016, Le Friant et al., 2020; **Figure 1B**). The deformation microstructures in cores U1399 and U1400 range from brittle to ductile and polyphasic (mixed), with inclined or contorted beds in highly variable degrees and directions. They are acquired after sediment deposition and may be the result of multiple successive but independent episodes of stress (Hornbach et al., 2015; Brunet et al., 2016). Laboratory experiments and numerical models show that lower permeability and high fluid pore pressures exist in some discrete units in the core, where slight changes in the stress regime may have triggered motion and local deformation (Lafuerza et al., 2014; Hornbach et al., 2015). A comprehensive model of emplacement of the debris avalanches and associated submarine landslides was proposed combining data of the IODP 340 expedition and geophysical data of three cruises (AGUADOMAR held in 1999, CARAVAL held in 2002 and GWADASEIS held in 2009; see Deplus et al., 2001; Le Friant et al., 2003; Brunet et al., 2016): the overload generated by the accumulation of debris flows produced by flank collapses at the break in slope on the seafloor triggers the sliding of pre-existing sediments along décollement surfaces and induces deformation of high-pore pressure units distributed within the submarine landslide thus created (Le Friant et al., 2015; Brunet et al., 2016; Le Friant et al., 2020). Core U1399 is less deformed than core U1400 and contains a large section of undeformed well-bedded sediments at the top. The existence of such undeformed layers at the top of the SLDs in all cores shows that deformation stopped over 50 ka ago (Brunet et al., 2016; Le Friant et al., 2020; **Figure 3**). Site U1399 is close to the site GS 2 of the 1976 cruise Gs7605 (Carey and Sigurdsson, 1980; Reid et al., 1996; **Figure 1B**).

3 MATERIALS AND METHODS

Cores U1397A and U1399A are simultaneously studied in this research to complete the chronostratigraphic information available in published studies on land and in marine cores and make an attempt to interpret the distal deposits of SLDs.

3.1 Lithostratigraphic Facies Analysis

At the studied sites, the sedimentary units consist of various combinations of hemipelagic sediments, tephra fall deposits, turbidites (bioclastic and volcaniclastic), debris flow deposits, and homogenized sandy-mud lithofacies (both referred here as debrites). The distinction between the different sedimentary facies is often a complex task due to their large variability and numerous artifacts due to piston coring (Cassidy et al., 2014; Jutzeler et al., 2014). Therefore, we use the nomenclature defined on-board and reported in the visual core descriptions (VCDs, Le Friant et al., 2013). Detailed descriptions and interpretations of these lithostratigraphic facies can be found in the studies by Talling et al. (2012), Trofimovs et al. (2013), Cassidy et al. (2014), Coussens et al. (2016a), Jutzeler et al. (2017) and for cores offshore Martinique in the studies by Le Friant et al. (2013),

Lafuerza et al. (2014) Brunet et al. (2016), and Le Friant et al. (2020). The distinction between turbidites and tephra layers, critical for the current investigation, is not always straightforward. Tephra layers consist of thin (centimeter to tens of centimeter) and fine grained (<1 cm) deposits either well-sorted and normally graded or massive with sharp contacts with sediments. They contain different types of volcanic clasts and separated minerals. The content in biogenic and other non-volcanic material is <10%. Different types of tephra deposits have been defined on-board based on deposit characteristics (fallout or volcaniclastic deposit) and nature of volcanic fragments (pumice, black scoriae, dome fragments, and separated minerals). The most frequent types are pumice clasts and separated minerals (mainly plagioclase and, to a lesser extent, pyroxenes and more rarely amphibole, biotite, olivine, or quartz). Glass shards are almost absent. Laboratory analysis of tephra layers identified on-board in the upper ~10 m of the core U1397A indicates that most of them (~60%) actually contain more than 50% of fresh pumice clasts and/or scoriae and separated minerals, but ~20% are not of direct volcanic origin but are remobilized deposits, for example, in some turbidites (Del Manzo et al., in prep). Here, we use on-board identifications of tephra layers, with some addition or exclusion after careful examination of VCDs. No attempt has been made to distinguish the different volcanic or magmatic types which require much more detailed investigations (Del Manzo et al., in prep) that are beyond the scope of this study.

The volcaniclastic turbidites have similar lithology and are also normally graded (segregation and sorting) by transport in the sea, but they are generally much thicker (tens of centimeter to tens of meter) and contain much coarser fragments (>1 cm). Pumice clasts most frequently represent the highest volcanic fraction. They are sometimes marked by an erosive base and may incorporate a significant fraction of pre-existing sea floor sediments. Volcanoclastic turbidity deposits may result from pyroclastic density currents (mainly pumice flows) entering into the sea or from remobilization of pyroclastic deposits on the submarine slopes or on land (Cassidy et al., 2014; Jutzeler et al., 2017). Debrites are deposits of submarine flows of debris avalanches. Homogenized muddy sand layers observed in some IODP 340 cores could not only result from mixing of pre-existing stratigraphy within the localized zones of intense shear (Brunet et al., 2016) but can also represent distal deposits of submarine debris flows (Talling et al., 2010; Talling, 2013; Talling, 2014).

3.2 Biostratigraphy

Planktonic foraminifers collected on board in both cores are characteristic of Upper Miocene to Upper Pliocene (Le Friant et al., 2013). An overall trend to older material with depth is observed in core U1397A, with an age younger than 220 ka for the top 25 m, younger than 250 ka from ~50 to 100 m, and younger than ~350 ka from ~100 m to ~400 ka at the bottom of this site (Le Friant et al., 2013). In core U1399A, the same fossils were only found in low numbers, and no reliable planktonic foraminiferal data were found.

3.3 Chronostratigraphy: $\delta^{18}O$ Measurements and ^{14}C Dating

The combined use of ^{14}C dating and variations of oxygen isotopes of marine foraminifers makes it possible to establish a reliable chronostratigraphy of marine sediments (Keller et al., 1978; Paterne et al., 1986; Lowe 2011; Griggs et al., 2014; Lowe 2014). *Globigerinoides ruber* was collected in hemipelagic layers of both cores for $\delta^{18}O$ analyses (611 in the upper 95 m of U1397A and 911 in the upper 150 m of U1399A). The collection was as systematic as possible at a depth interval ranging between 2 and 20 cm depending on lithology, with a mean interval of ~10 cm. Stable oxygen isotope analyses were carried out at the Laboratory ISTeP (Institut des Sciences de la Terre de Paris, Sorbonne-Université, Paris, France). No chemicals were used to disaggregate the sediments, and at all stages in the processing, deionized water was used to ensure no dissolution of the carbonate microfossils. The samples were sieved by washing on a stainless steel sieve and slowly dried at 35–40°C. Pristine test samples of white and pink *Globigerinoides ruber* > 150 μm in size were picked (~10 mg) and sonically cleaned. The samples were reacted with 100% H_3PO_4 acid under vacuum in a Kiel IV automatic preparation device at 70°C, and the resulting CO_2 was analyzed using a ThermoFisher Delta V Advantage IRMS mass spectrometer. Oxygen isotope values ($\delta^{18}O$) are reported as per mil (‰) deviation in the isotope ratio ($^{18}O/^{16}O$) standardized to the Vienna Peedee belemnite—VPDB scale using an internal standard (Marceau marble: $\delta^{18}O$ = −1.83‰ V-PDB) calibrated against NBS-19 using the classical method. The analytical reproducibility (1σ) on replicate analyses was 0.1‰. The mean bulk reproducibility is ~0.27‰. It includes the variability in sampled sediment and was estimated from two to three replicates in ~40 sediment layers of core U1397A. $\delta^{18}O$ data are reported in **Supplementary Tables S1A,B**.

For ^{14}C dating, approximately 800 specimens (~10 mg) of *G. Ruber* of a size >150 μm were picked in each of the selected hemipelagic sediment layer. AMS analyses were performed by Artemis National Platform LMC14 (CEA Saclay, Gif sur Yvette, France) or by Beta Analytics Inc. (FL, United States, www.radiocarbon.com) using their in-house protocols. Thirteen samples were selected in the upper 7 m of U1397A and seven samples in the upper 3 m of U1399A. ^{14}C dating results are reported in **Supplementary Tables S2A,B** as conventional radiocarbon years BP, expressed at the ±1σ level for overall analytical confidence. The AMS dates are calibrated against the Marine13 dataset using CALIB 7.0 Radiocarbon Calibration software (Stuiver and Reimer, 1993; Reimer et al., 2013a; Reimer et al., 2013b).

4 RESULTS

4.1 Lithology, Deformation, and Seismic Facies of Cores U1397A and U1399A

Simplified lithology (hemipelagic sediments, tephra layers, turbidites, and debrites) and possible deformation figures established on board from visual core descriptions (VCD's; Le

Friant et al., 2013) are compared to seismic facies (Brunet et al., 2016) for both cores in **Figure 3**. For interpretation of the stratigraphic sections reported in **Figure 3**, high-resolution logs are reported in **Supplementary Figure S1**.

4.1.1 Site U1397

Two holes have been cored on this site (**Figures 1B**, **3A**). The top 50 m of core U1397A contains a slightly higher proportion of tephra and hemipelagic sediments and a lower proportion of turbidites than in core U1397B distant about 15 m to the south (see **Supplementary Figure S2**). The general distribution of hemipelagic and tephra layers is, however, similar. This indicates that turbidity currents are strongly channelized and may partially and superficially erode pre-existing sediments. The core U1397A (Lat 14°54.4081N, Long. 61°25,3530W, water depth 2,482.2 m) reached 265.5 m bsf (meters below sea floor), but only the uppermost 120 m has good recovery. Seismic data indicate that at least the upper 90 m of the core penetrates regular reflectors that correspond to undisturbed well-bedded sediments; below, numerous chaotic reflectors are visible. At least 300 tephra layers have been recognized in the top 50 m. Numerous thick turbidites are intercalated between thick well-bedded sediment layers in the intervals ~50–65 m, ~95–120 m, and below 140 m bsf. Six different lithostratigraphic units (A to H) are recognized (**Figure 3A**). Unit A (0–28 m bsf) comprises a sequence of hemipelagic sediments with interbedded tephra layers and few thin and poorly sorted turbidites. Unit B (28–53 m bsf) comprises the same material but with numerous volcaniclastic turbidites, particularly in the upper 5 m. Unit C (53–76 m bsf) is mainly a turbidite sequence of mixed (bioclastic–volcaniclastic) composition. Turbidites are normally graded and contain variable amounts of fresh pumice. The turbidite layers are most often in direct contact with no separating hemipelagic layer. The basal zone of unit C (<3 m thick) contains a debrite and a section of deformed sediment. Unit D (76–91 m bsf) comprises a series of volcaniclastic turbidites (more abundant from ~83 m bsf) and a few tephra layers which are interbedded in a hemipelagic mud. The proportion of hemipelagic sediment is lower than that in unit C. Unit E (91–120 m bsf) comprises a series of thick massive to normally graded volcaniclastic turbidites containing a large amount of massive to poorly vesiculated lava fragments. Below ~120 m bsf, the core recovery was very low, and the stratigraphy is uncertain. The recovered sediments are significantly and increasingly compacted from this depth. Three different units were successively sampled: 1) between ~150 and ~170 m, two sequences of hemipelagic sediments weakly compacted at the top with a progressive lithification into mudstones with depth; 2) between ~170 and 230 m bsf, many sequences of mud-rich sandstone layers and semi-consolidated, highly fractured, and contorted mudstones with abundant lava clasts, few pebbles, and a larger block comprising andesitic lava containing large phenocrysts of amphibole and quartz; 3) between ~230 and ~265 m bsf, a sequence of heavily bioturbated hemipelagic mud with few interbedded layers of bioclastic sandstone.

4.1.2 Site U1399

Site U1399A (Lat 14°23,2419N, Long. 61°42,6833W, water depth 2,900.8 m) reached 274.7 m bsf (**Figures 1B**, **3B**). Cored sediments are dominated by a combination of hemipelagic mud with interbedded tephra and volcaniclastic turbidites and various types of deformed sedimentary intervals that occur at different depths. Some units contain debrites. Seismic data indicate a thick zone (~25–150 m bsf) with chaotic reflectors intercalated between two zones with typical well-bedded facies (0–25 m bsf, and below ~150 m bsf, **Figure 3B**). The chaotic facies correspond to locally highly deformed sediments. Eight different lithostratigraphic units (A–H) are defined based either on changes in the cored material characteristics or a distinct marker layer (Le Friant et al., 2013; **Figure 3B**). Unit A (0–24 m bsf) mainly comprises hemipelagic mud with abundant tephra layers and several small turbidites. Unit B (24–50 m bsf) is a sequence of variably deformed and contorted hemipelagic sediment and debrites with a muddy sand matrix. Unit C (50–72 m bsf) consists of hemipelagic mud with interbedded tephra layers and thin turbidites (<1 m thick). The base of unit C comprises a 1-m-thick interval of hemipelagic mud overlain by a thick turbidite (~8 m). Unit D (72–80 m bsf) comprises highly deformed sediments in the upper part and weakly deformed hemipelagic mud in the lower part. Unit E (80-112 m bsf) consists of a succession of alternating layers of undeformed hemipelagic mud with interbedded tephra layers and thin turbidites, deformed pelagic mud, debrites, and turbidites. Unit F (112–150 m bsf) comprises a sequence of highly deformed and contorted hemipelagic sediment with turbidites and contorted tephra layers. Unit G (150–192 m bsf) comprises sequences of pumice-rich turbidites with few interbedded hemipelagic mud and tephra layers. Unit H (192–270 m bsf) has very low recovery and consists of hemipelagic mud with interbedded tephra layers and pumice-rich turbidites.

4.2 Chronostratigraphic Data and Model Ages

The patterns of $\delta^{18}O$ vs. hemipelagic sediment thickness compared to standard $\delta^{18}O$ vs. age curves allows to establish the age ("model age") of hemipelagic sediments as a function of depth in the core. The mean time resolution (±1σ) of the chronological reconstructions is theoretically ~1 ka for U1397A and ~4 ka for U1399A, as estimated from the mean sedimentation rates and sampling interval (~10 cm). In many cases, however, (no recovery, gaps in hemipelagic sedimentation), the age can only be bracketed in a much larger time interval. The large differences between the $\delta^{18}O$ depth patterns of U1397A and U1399A are due to differences in both sedimentation rates and post deposition perturbations (mass transport, deformations etc.).

4.2.1 Core U1397A

Lithology of core U1397A is compared to the $\delta^{18}O$ patterns in **Figure 4**. $\delta^{18}O$ data obtained at approximately the same depth resolution in two other cores drilled near site U1397 (**Figure 1B**) are also reported for comparison: the ~10-m-long core CARMAR 4

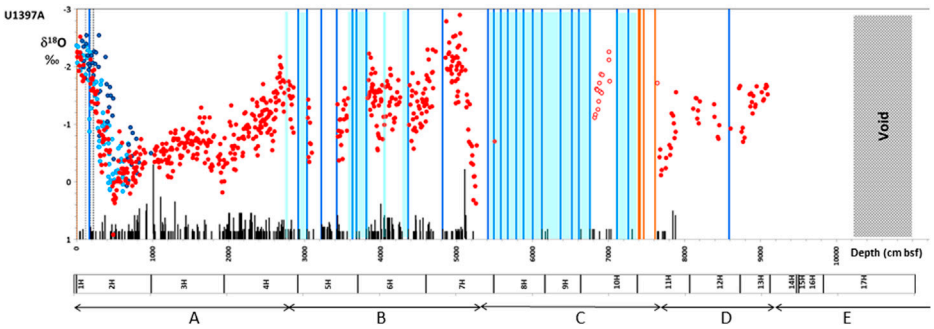


FIGURE 4 | Synthetic logs and $\delta^{18}O$ values of core U1397A. Comparison with cores U1401A and CARMAR-4. $\delta^{18}O$ data: red dots U1397A; light blue dots: CARMAR-4 (Boudon et al., 2013); dark blue dots: U1401A (Solaro et al., 2020). Blue domains: turbiditic zones; blue bars: turbidites >50 cm; black bars: tephra units; orange bars: debrites. The height of the bars relates to the relative thicknesses of the deposits. Gray domains: void in core; dots: $\delta^{18}O$ values; open circles: series of samples of which the $\delta^{18}O$ pattern is not consistent with the stratigraphic position in the core. They correspond to sedimentary units displaced by submarine sliding ("duplicate units"). Letters are the different core section labels and lithological units (see **Figure 3A**).

(Boudon et al., 2013) and the ~15-m-long core U1401A (Solaro et al., 2020). The three datasets are consistent in absolute values and dispersion, indicating that the relatively high dispersion of $\delta^{18}O$ values is mainly due to the natural heterogeneity of sediments rather than analytical. This natural heterogeneity is likely due to the sedimentation conditions in an agitated marine environment on steep volcano slopes. $\delta^{18}O$ data for U1401A display a slightly higher dispersion than those for U1397A, though performed in the same conditions (**Figure 4**): it is likely due to its location at the outlet of Mt Pelée collapse structures, leading to significant disturbance of the sedimentation (**Figure 1B**).

$\delta^{18}O$ data of core U1397A display a continuous trend over the upper 28 m of the core (unit A). Below, the $\delta^{18}O$ record is discontinuous due to the abundance of thick turbidite layers or poor recovery (**Figure 4**). The $\delta^{18}O$ pattern over the upper 28 m reproduces the typical isotopic variations since the last interglacial low-stand to the present day, with maximum $\delta^{18}O$ values at ~18 ka. The age–depth calibration is estimated using both ^{14}C dating and $\delta^{18}O$ measurements (see **Supplementary Tables S1A, S2A**). Due to the volcanic environment and the proximity to the coast, the sedimentation may be disturbed by volcanic events (such as large eruptions, volcaniclastic turbidity currents, or debris avalanches) or climatic events (such as strong floods or storms). These events may be considered instantaneous compared to the time resolution, and their deposits can be relatively easily identified. Due to relatively low frequency of such events and the low thickness of volcaniclastic layers in the upper 28 m of the core, we assume in first approximation a constant hemipelagic sedimentation rate. The thickness of hemipelagic sediments is estimated by subtracting the thickness of volcanic (VL), turbidite (Tu), or debrite (D) layers as reported in the VCD from the depth in core (see **Supplementary Table S1A**). Then, the use of ^{14}C dating (**Supplementary Table S2A**) leads to a mean sedimentation rate of ~23 cm/ka (**Figure 5A**). This rate is lower (~9–10 cm/ka) for the upper meter of the core, but then increases rapidly. It may be due to coring under-recovery of the upper unconsolidated sediments. From this first estimate, a new mean sedimentation rate is obtained (**Figure 5B**) by fitting "by eye" the $\delta^{18}O$ pattern to a reference pattern derived from the following well-constrained $\delta^{18}O$ age curves (see **Supplementary Figure S3**): SPECMAP LR-04 (Lisiecki and Raymo, 2005), ODP999, and VM78-122 in the Caribbean Sea (Broecker W. et al., 1988; Broecker W. S. et al., 1988; Broecker et al., 1990) and CARMON-2 offshore Montserrat (Le Friant et al., 2008). A compaction factor k^0 to take into account for sediment pile overload is defined as follows: $Vs = Vs^0\ (1 - k^0\ d)$, where Vs^0 and Vs are, respectively, the actual and the apparent sedimentation rates and d is the depth expressed in centimeter (bsf). The best fit is obtained for $Vs^0 = 28$ cm/ka and $k^0 = 2.5{\cdot}10^{-5}$ cm^{-1} (**Figure 5A**). The calibration curve is consistent with that of core U1401A (Solaro et al., 2020) and with the hemipelagic sedimentation rates deduced from biochronology in cores En 46 and GS 27 cored near the Caribbean coasts of St Lucia and the Grenadines (Reid et al., 1996; **Figure 5A**).

Sediment erosion and sliding and doubling of sediment packages as discussed below inhibit application of the same fitting method to core sections older than 130 ka (**Figure 4**). In unit C (~53–76 m bsf) in core U1397A, the sediments mainly consist of a series of volcaniclastic turbidites, representing a total thickness of ~15 m ~ 2 m at 53 m, ~5.5 m at 55.5 m, ~4.5 m at 61.5 m, ~2 m at 66.5 m, and ~0.4 m at 70 m bsf (**Figure 4**). This sequence of turbidites lies on top of a debrite-like deposit between 74 and 76 m bsf. Only a ~1.6 m thick continuous sequence (68.4–70 m bsf) of hemipelagic sediments is preserved within the turbidite sequence. It displays a $\delta^{18}O$ pattern that is not consistent with possible nearby reference patterns, that is, older than 130 ka. This pattern is, however, similar to that of a shallower section (46–48 m bsf, in unit B), which corresponds to the 115–121 ka time period (**Figures 4**, **5B**). We assume that this sedimentary sequence is a duplicate unit and that its stratigraphic position is controlled by the emplacement of the complex system comprising thick turbidites and debrites of unit C (53 and 76 m bsf; **Figure 5B**).

To fit the $\delta^{18}O$ measured in the series of hemipelagic sediments of unit D (between 76.7 and 90.2 m bsf, the

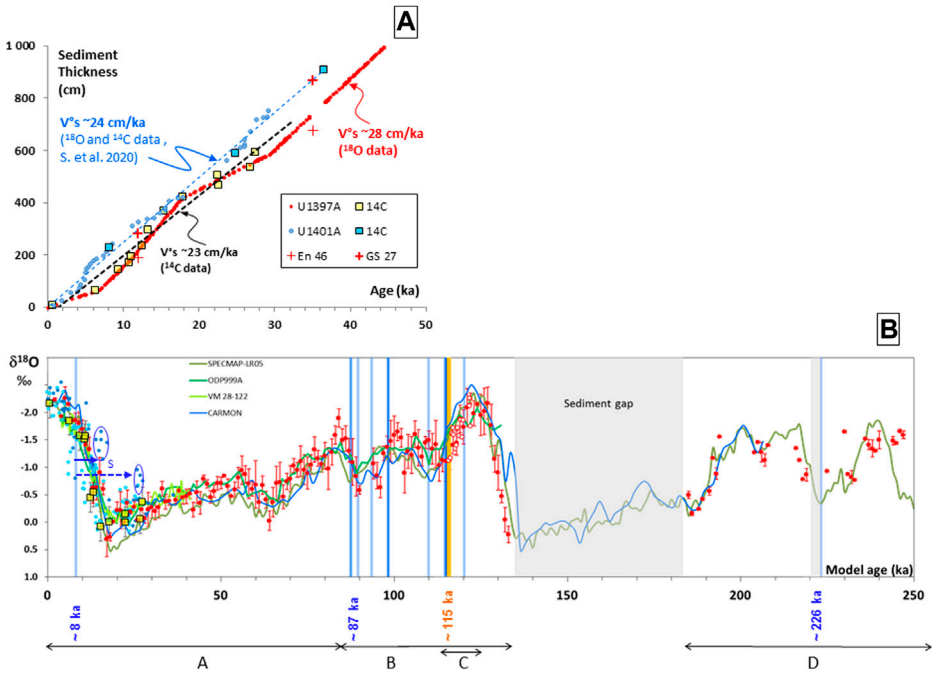


FIGURE 5 | Model age and sedimentation rate of core U1397A. Comparison with core U1401A. **(A)** Sedimentation rates: $\delta^{18}O$ data; red dots: U1397A; blue dots: U1401A (data from Solaro et al. (2020)). Squares: ^{14}C data; yellow: U1397A; blue: U1401A. V°_{S}: mean hemipelagic sedimentation rates. Crosses: data of cores En 46 and GS 27 (biochronology, two values per core; Reid et al., 1996; see also **Figure 8**). **(B)** Model age of core U1397A $\delta^{18}O$ data: red dots: U1397A (mean values with error bars for a sampling step of 1 cm); open red circles: sedimentary units displaced by submarine sliding ("duplicate units"); light blue dots: CARMAR-4 (Boudon et al., 2013); dark blue dots: U1401A (model age from Solaro et al., 2020); continuous green and blue lines: standard $\delta^{18}O$–age patterns (SPECMAP, ODP-999, VM 28-122, CARMON). Yellow squares: ^{14}C data (age errors are within symbol size). Blue bars: turbidites >50 cm; orange bars: debrites; gray domain: erosion or sedimentation gaps; open circles: duplicate hemipelagic unit. Blue ellipses: the two anomalous $\delta^{18}O$ patterns in core U1401A considered stratigraphically discordant units. Letters are the different lithological units (see **Figure 3A**). See also **Figure 4** and the text for further explanations.

maximum depth of $\delta^{18}O$ measurements, **Figure 4**) with the isotopic reference patterns, it is necessary to assume a large gap of hemipelagic sediments at the base of unit B (from 53 m bsf), which corresponds to the turbidites of unit C (**Figure 4**). The missing sediments correspond to a time period of ~50 ka (between 135 and 185 ka; **Figures 5A,B**) and theoretical thickness of hemipelagic sediments of ~14 m estimated from the hemipelagic sedimentation rate. Another but smaller sedimentation gap likely exists at ~85.8 m (in unit D) and is also contemporaneous (at ~226 ka) of a ~1.5 m-thick turbidite. The overall fit with isotopic reference curves for the time period 185–250 ka is less satisfactory than for shallower sediments. The core U1397 provides the longest time interval (~1–133 ka) of continuous sedimentation collected offshore Martinique. The $\delta^{18}O$ record and the corresponding model ages are wholly consistent with those of the CARMON 2 piston core offshore SW Montserrat (**Figure 5B**), which records a continuous sedimentation over ~250 ka, but with much lower sedimentation rates (~2–4 cm/ka; Le Friant et al., 2008).

4.2.2 Core U1399A

Lithology and $\delta^{18}O$ measurements of core U1399A are compared in **Figure 6**. Site U1399A is located further from the coast (~70 km) and at a much greater water depth (2,900 m) than site U1397A (located at ~20 km and 2,480 m water depth), but far from the main marine streams: the mean hemipelagic sedimentation rate should be much lower. Because the U1399A core was drilled through the SLDs, it contains numerous turbidites and debrites and intense deformation over large depth intervals that are related to the volcanic activity and flank collapses of Mt Pelée and possibly Pitons du Carbet (**Figure 3B**). Large perturbations in the hemipelagic sedimentation record are expected. Of the seven ^{14}C dates performed in this core, only three are below the upper age limit of the method (<45 ka; **Supplementary Table S2B**). At the top of unit A, there is a large gap between the ^{14}C dates (~25 ka; **Supplementary Table S2B**) of the two hemipelagic sediment layers 1H1 80-82 and 1H2 60-62 (at depths 82 and 212 cm bsf, respectively), which bracket a 1.2-m-thick turbidite (vertical gray arrows in **Figure 6A**). In the nearby site GS 2, a coarse pyroclastic deposit (75-cm thick) was also reported at a similar depth and attributed to the volcanic activity of Dominica (Reid et al., 1996). The different ^{14}C dates obtained in sediments collected below this turbidite (>210 cm bsf, unit A; **Supplementary Table S2B**) are inconsistent, even considering the large age uncertainties (**Figure 7A**). The existence of a thick turbidite and chaotic distribution of ^{14}C dates in sediment layers below it argue in favor of a strong disturbance of the original sedimentary pile below 80 cm bsf.

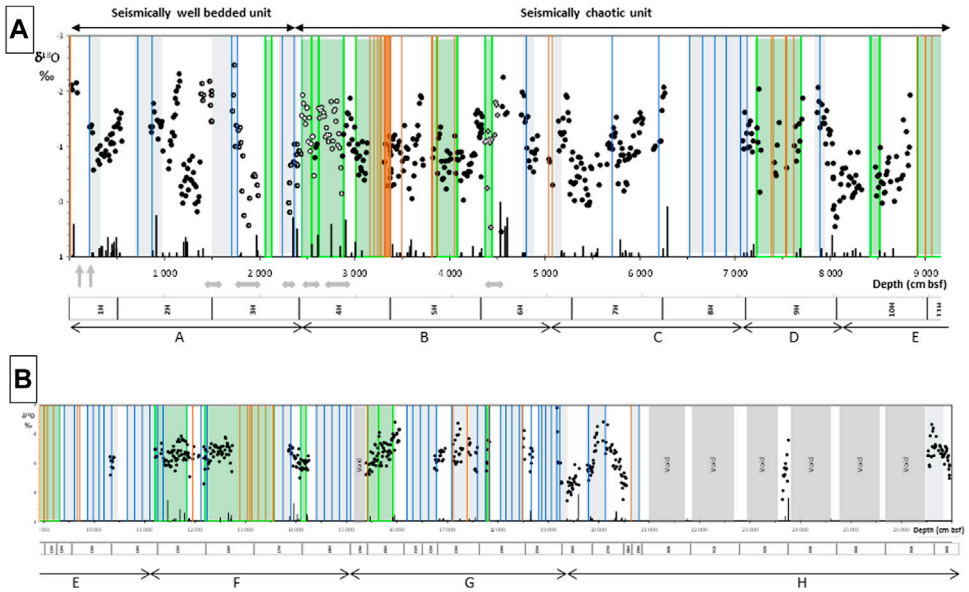


FIGURE 6 | Synthetic logs and $\delta^{18}O$ values of core U1399A. **(A)** 0–90 m bsf. **(B)** 90–270 m bsf. $\delta^{18}O$ data: dots U1399A; open circles: sedimentary units displaced by submarine sliding ("duplicate units"). Blue domains: turbiditic zones; blue bars: turbidites >50 cm; black bars: tephra units; orange bars: debrites. The height of the bars relates to the relative thicknesses of the deposits. Green domains: deformed zones; gray domains: void in core. Gray arrows: the horizontal arrows indicate the duplicate units, and the vertical arrows indicate the first two sediment gaps identified in the upper part of the core (they correspond to the gray domains in **Figure 7A**; see the text for further explanations). Letters are the different core section labels and lithological units (see **Figure 3B**). The reader is referred to high-resolution figure on the web version of this article for benefit.

The $\delta^{18}O$ patterns of the next 2.5–4.2 m in core U1399A (**Figure 6A**), and of the 12.5–17.5 m in core U1397A (base of unit A; **Figure 5B**), are similar and correspond to the age range ~43–60 ka (**Figure 7A**). This confirms the existence of a large sediment gap corresponding to the age range ~12–43 ka and equivalent to ~1.5 m of hemipelagic sediments in core U1399A (gray domain in **Figure 7A**). The few significant ^{14}C data (layers shallower than 80 cm bsf, **Figure 7B**) provide a rough estimate of the hemipelagic sedimentation rate $Vs^0 \sim 9$ cm/ka. This value is consistent with the biostratigraphic estimate of Vs°~8 cm/ka at the site GS 2 nearby (Reid et al., 1996). As for the core U1397A, a compaction factor of $k^0 = 10^{-6}\,cm^{-1}$ is estimated from the comparison of the first well-identified continuous sediment units. The fit of the $\delta^{18}O$ pattern of core U1399A with reference isotopic curves over the last 150 ka (**Figure 7A**) provides a more confident estimate of the mean hemipelagic sedimentation rate of ~5.2 cm/ka (**Figure 7B**).

For greater depths, we investigate step by step, with increasing depth, the different continuous series of hemipelagic sediments using the VCDs (**Figure 6**). The $\delta^{18}O$-age pattern of each continuous series is established using the estimate of the hemipelagic sediment thickness and mean sedimentation rate. As for core U1397A, these patterns are compared and fit to reference isotopic curves considering possible duplicates or gaps in the sedimentary sequence. Duplicates and gaps are generally bracketed by thick turbidite, debrite, or deformation zones (**Figure 6**). In deformed zones, the actual thickness of sediments is lower than that measured by depth variations because of folding or tilting of the sedimentary layers. The apparent sedimentation rate is $Vs = Vs^0\ (1 - k^0\ d)\ k^1$, with $k^1 > 1$. For all deformed zones, we adopted, in first approximation, an elongation factor of 10%, let $k^1 = 1.1$, which is consistent with observations (Lafuerza et al., 2014; Brunet et al., 2016).

The resulting age model for the core section down to 210 m bsf is reported in **Figure 7C**. The consistency between the SPECMAP curve and the $\delta^{18}O$ model age of U1399A is relatively satisfying up to ~1.2 Ma (~120 m bsf). Beyond this, especially for ages >1.6 Ma (>190 m bsf), the poor recovery, the scarcity of continuous sedimentary piles and the almost systematic deformation prevent confident fitting. On the basis of $\delta^{18}O$ patterns, many duplicate units are identified in the upper 45 m of the core (base of unit A and the whole unit B; **Figures 6**, **7C**); they probably also exist at greater depths in the sediments but are not identifiable. The origin of such chronological discrepancies will be discussed below in the context of stratigraphic disturbances caused by erosion and sliding sediment packages. The decrease in the amplitude of $\delta^{18}O$ variations for ages older than 1 Ma is well-known (Mid-Pleistocene transition; see, for example, Clark et al., 2006) and consistent with the $\delta^{18}O$ patterns between ~95 and 175 m bsf (units E and F; **Figures 6B**, **7**). On the contrary, the $\delta^{18}O$ pattern between 195 and 210 m (unit H; **Figure 6B**) is characterized by a broad peak with large variations in $\delta^{18}O$ values (range: [−2.5; 0.3‰]), which is inconsistent with ages older than 1 Ma. This range of $\delta^{18}O$ values is typical of the time periods 0–250 ka or 350–750 ka, which suggests that this sediment package could represent a 10-m-thick duplicate unit of a relatively recent material overlain by a very thick pile of at least 100 m of older sediments.

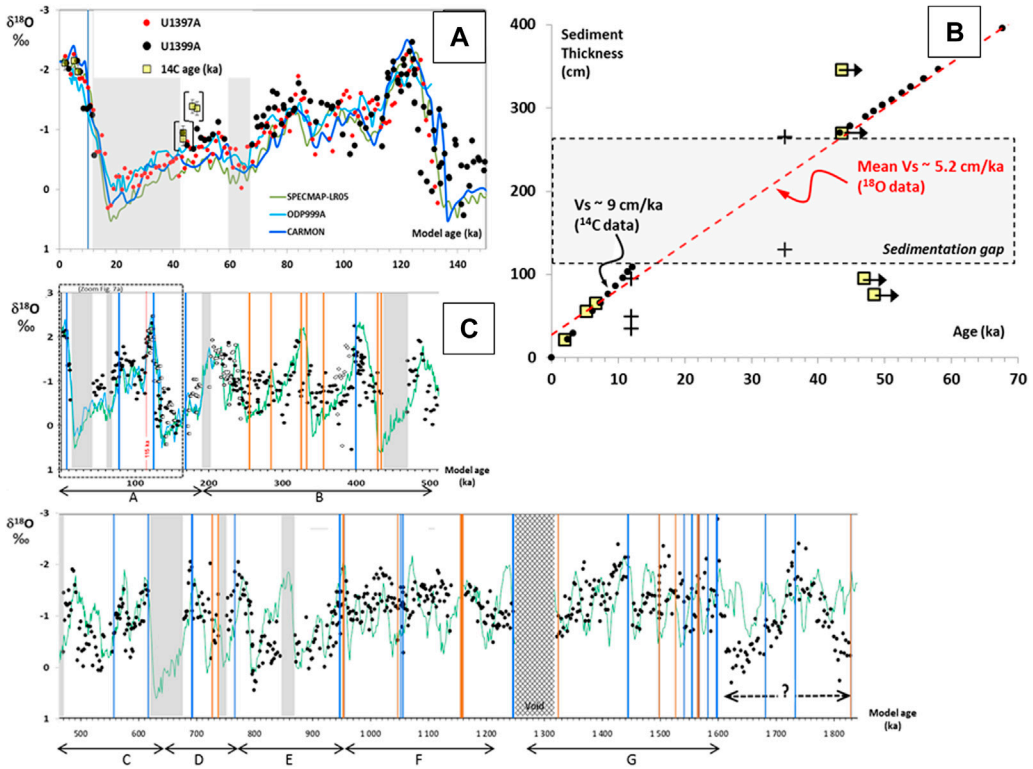


FIGURE 7 | Model age and sedimentation rate of core U1399A. **(A)** Model age for the time period 0–150 ka. Dots: $\delta^{18}O$ data of cores U1399A (black) and U1397A (red). Squares: ^{14}C data of core U1399A; error bars are within symbol size; black arrows: data out of ^{14}C dating range. Continuous lines: standard $\delta^{18}O$—age patterns. Blue bars: turbidites >50 cm; orange bars: debrites. Gray domain: erosion or sedimentation gaps (identified by arrows in **Figure 6A**). **(B)** Sedimentation rate. Black dots: U1399A; squares: ^{14}C data. V°_{S}: mean hemipelagic sedimentation rates. Crosses: data of cores En 6, GS 2 and GS 18 (biochronology, Reid et al., 1996; see also **Figures 1**, **8**). **(C)** Model age for the time period 0–1.8 Ma. $\delta^{18}O$ data: black dots; open circles: sedimentary units displaced by submarine sliding ("duplicate units"). Reference curves: SPECMAP (green) and CARMON (blue). Other symbols as in **(A)**. Letters are the different core section labels and lithological units (see **Figure 3B**). For ages older than ~1 Ma, the proposed chronology has a low confidence due to large deformation and low recovery. No attempt has been made to interpret data for sediments deeper than 200 m (i.e., older than >1.6 Ma).

5 DISCUSSION

5.1 Preservation of Sedimentary Deposits and Chronostratigraphy

The Caribbean flank of the southern part of the Lesser Antilles Arc is characterized by high sedimentation rates of both hemipelagic and volcanic origin. The volcanic supply is high and variable along the Caribbean coasts because of the distribution of the active volcanic centers on the western side of the islands and of the western vergence of the horseshoe-shaped structure generated by flank collapses that channel the pyroclastic flows and debris avalanches (**Figure 1**; Deplus et al., 2001). The distribution and thickness of volcaniclastic turbidites and debrites are also extremely variable as indicated by the VCDs of the different cores offshore Martinique (**Figure 3**; Le Friant et al., 2002; Le Friant et al., 2013). Two factors favor erosion of the sedimentary deposits: 1) the local sea floor morphology with very steep submarine slopes and deep canyons related to regional and local fracturing (Feuillet et al., 2002) which favor the sliding of sediment piles and erosion by powerful turbidity currents, and 2) the volcanic activity itself through potentially erosive debris avalanches and related submarine landslides (Le Friant et al., 2015; Le Friant et al., 2020). On the contrary, on the eastern (Atlantic) side of the islands, the hemipelagic and volcanic sedimentation rates are much lower (Reid et al., 1996; Le Friant et al., 2008), and volcanic deposits almost exclusively consist of small volcanic clasts transported in volcanic plumes, but the preservation of sediments over long periods of time is much better (Reid et al., 1996).

The hemipelagic and volcanic sediments recorded in cores offshore Martinique generally consist of a series of continuous and well-preserved units of highly variable thicknesses (from typically 10 m–50 m, but sometimes some meters only) separated by volcaniclastic turbidites or more rarely by debrites. No erosion features at the top or the bottom of these units are identified in VCDs (Le Friant et al., 2013), but a fine analysis of $\delta^{18}O$ patterns suggests that some rare debrites may have had a significant erosive effect as, for example, at ~50 m bsf in core U1399A (unit C, 435 ka; **Figures 6**, **7C**). All along the core U1399A (**Figure 7C**) and below ~52 m bsf in core U1397A (**Figures 4**,

5B), many large hemipelagic sedimentation gaps are identified through $\delta^{18}O$ chronostratigraphy. Finally, numerous duplicate sedimentary units are also identified in core U1399A (**Figure 6A**) and one in core U1397A (unit C and following; **Figure 4**) that result from slumping of coherent sediment slices down steep canyon flanks (U1397A) or at the front of large submarine landslides (U1399A). Thus, the sedimentary records of both cores reflect continuous hemipelagic sedimentation with discrete volcanic deposits, turbidites, and more rarely debrites producing sedimentary piles that are periodically destabilized or eroded. Potential triggering processes are various: sediment overload and slope failure, large volcanic events or flank collapses (Le Friant et al., 2015; Brunet et al., 2016; Le Friant et al., 2020), earthquakes, etc.

Three factors affect the $\delta^{18}O$ correlations and age models: inconsistent $\delta^{18}O$ values (i.e., duplicates), sediment gaps (by erosion), and recovery gaps. The continuous hemipelagic sediment record in the upper 28 m (Unit A) of core U1397A allows the reconstitution of a precise chronostratigraphy over ~135 ka in both cores (**Figures 5B**, **7A**). On the basis of reference $\delta^{18}O$ age curves, the age resolution is ~2 and ~5 ka in cores U1397A and U1399A, respectively (see **Supplementary Figure S3**). In core U1399A, this reconstitution is possible up to ~1.5 Ma but with a much lower age resolution and large discontinuities especially from ~450 ka; poor recovery, erosion, and slumping and deformation of sediments strongly affect the age model. All events recorded by well-identified deposits can then be dated. Tephra layers, despite some evidences of post-deposition transport on short distances, do not significantly disturb the hemipelagic sedimentation and are accurately dated. Since volcaniclastic turbidites and debrites are discontinuities in sedimentation, only maximum or minimum ages of emplacement can be estimated.

5.2 Sedimentation Rates

The hemipelagic sediments on the eastern side of the Grenada Basin consist of a dominant fraction of terrigenous (volcanic clay and silts) sediments supplied by island rivers and a low fraction of pelagic sediments produced *in situ* but also transported from the Atlantic Ocean by the powerful submarine currents through island passages (South Dominica, South Martinique, and South St Lucia; Reid et al., 1996; **Figure 8A**). In the Caribbean Sea, along the western coasts of the Lesser Antilles Arc, the hemipelagic sedimentation rates are variable in space and time; they are high close to the islands at the mouth of inter-island submarine channels and rapidly decrease away into the Grenada Basin (Reid et al., 1996). The pure hemipelagic sedimentation rates measured close to the shore (~25 km) in cores CARMAR-4 (upper 7 m; Boudon et al., 2013), U1401A (upper 8 m; Solaro et al., 2020), and U1397A (upper ~25 m) are similar, varying between 24 and 28 cm/ka (**Figure 5A**). The location of sites CARMAR-4 and U1397A at the mouth of the Dominica channel explains their slightly higher hemipelagic sedimentation rates than those of U1401A (**Figure 8A**). The sedimentation rates decrease rapidly with distance from the Grenada Basin with a mean value of ~5.2 cm/ka at ~70 km (site U1399A; **Figure 7B**). These low sedimentation rates are consistent with biostratigraphic estimates in the Grenada Basin (e.g., 8 cm/ka at site GS 2; Reid et al., 1996; **Figure 8A**). More generally, they are consistent with estimates in most sites in the Lesser Antilles Backarc, Forearc, or Volcanic Platform ranging between 2 and 8 cm/ka for at least the last 80 ka (Reid et al., 1996, **Figure 8A**). They are also consistent with recent estimates (3–4 cm/ka) using $\delta^{18}O$ and ^{14}C chronostratigraphy on cores offshore SW Montserrat (CARMON-2, Le Friant et al., 2008; U 1396, Wall-Palmer et al., 2014; Fraass et al., 2017; **Figure 8A**). The background hemipelagic sedimentation rates are, thus, generally <8 cm/ka in the whole east Caribbean Sea except along the flanks of the southern islands (sites U1397A and U1401A offshore Martinique and En46, ~60 km S offshore St Lucia) and in site GS-27, 220 km SW-offshore Grenadines, where they are 3–4 times higher (**Figure 8A**). The distribution of these sites suggests that the most active volcanoes in the southern Antilles Arc provide a higher supply of volcanic silts and clays and that there is an active transport of terrigenous sediments by the N–S surface coastal currents in the south Grenada Basin. Finally, there is no evidence of large variations in the hemipelagic sedimentation rate during the last glacial period in cores U1397A and U1401A (**Figure 8B**). This is consistent with the study of Reid et al. (1996) showing that in the southern part of the Antilles backarc, hemipelagic sedimentation rates are weakly dependent on sea level height, contrary to those in the northern regions.

The variations in sedimentation rates (in cm/ka) of every type of sediment (hemipelagic, volcanic, turbidites, and debrites) are estimated using model ages and sediment thicknesses corrected, if necessary, for deformation and discarding duplicate units (**Figure 8B**). Though some significant biases may occur for core U1399A due to underestimation of duplicate units and large chronology uncertainties for ages >450 ka, some robust observations can be highlighted. In both cores, hemipelagic sedimentation is largely dominant (~70% in U1397A and ~50% in U1399A). In core U1399A, sedimentation rates of volcaniclastic turbidites and debrites are largely dominant over those of tephra. In core U1397A, the turbidites and tephra sedimentation rates are similar. In core U1397A, the total sedimentation rate of ~43 cm/ka is roughly constant over the last ~150 ka (**Figure 8B**). The sedimentation rate of turbidites is highly variable and dominated by some discrete major events in a short interval of time between 90 and 120 ka (unit C; **Figure 8B**). In core U1399A, the total sedimentation rate is ~11 cm/ka over the last 1.5 Ma, and the sedimentation rates of turbidites and debrites are highly variable in time. All these observations are consistent with the location of the two sites: U1397A is close to the coast but far from the outlet of flank collapse structures and, thus, collects a significant fraction of erupted products but a low fraction of volcaniclastic turbidites. Site U1399A is located on the submarine landslides far from the coast: it collects much less volcanic tephra but is supplied by reworked material transported by submarine landslides and turbidity currents (Le Friant et al., 2020). Finally, no correlations exist between variations in sedimentation rates and changes in sea level, which suggests that volcanic products constitute the dominant supply of all types of sediment, which are therefore independent of sea level changes.

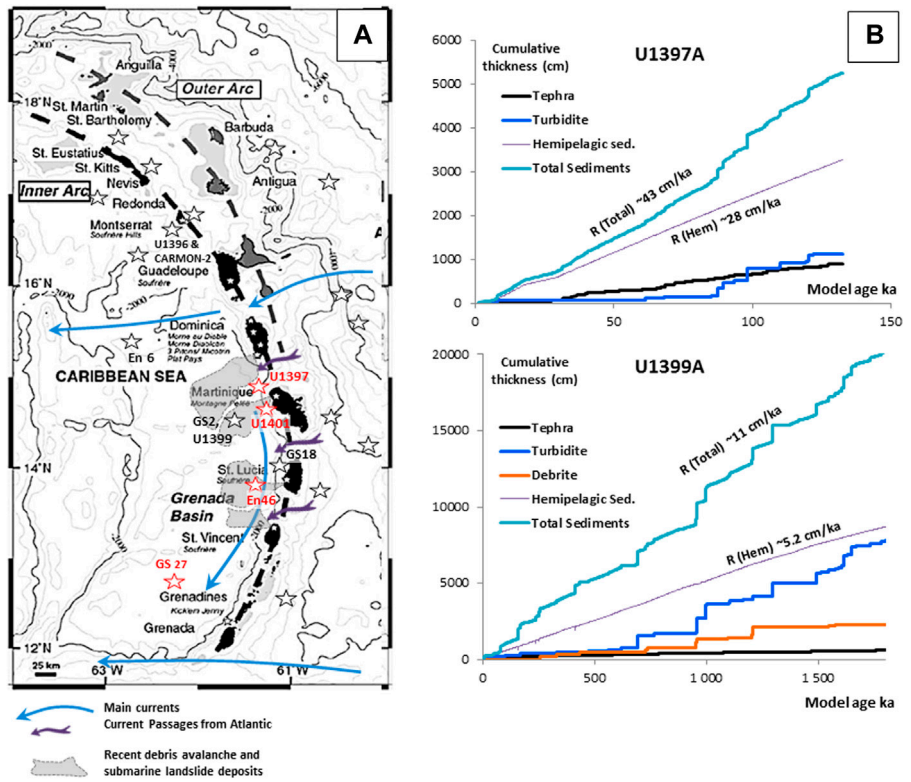


FIGURE 8 | Sedimentation rates. **(A)** Hemipelagic sedimentation rates in the South Caribbean Sea (Grenada Basin). Red stars: V˚s > 15 cm/ka; black stars V˚s < 8 cm/ka. Data sources: U1397A, U1399 (this work); U1401 (Solaro et al., 2020, modified); U1396 and CARMON-2 and NE Montserrat; Le Friant et al., 2008; Wall-Palmer et al., 2014 and Fraass et al., 2017); En 6, En 46, GS 2, GS 27, and other coring sites north Guadeloupe: biostratigraphic estimates (Broecker et al., 1990; Reid et al., 1996; Carey 1999). **(B)** Cumulative sediment thicknesses with time: sites U1397A and U1399A. R (Total) and R(Hem) values are the mean sedimentation rates of hemipelagic and total sediments. It is to be noted that hemipelagic curves are used as a reference (rates are estimated from ^{14}C and $\delta^{18}O$ dating for age <50 ka and beyond are assumed constant; see **Figures 5A**, **7B**).

5.3 Eruptive Activity

Depending on the eruptive style, volcanic deposits at sea are very variable in nature and thickness. Plinian and sub-Plinian eruptions producing pumice clasts and scoriae that are widely dispersed in the atmosphere are most likely to be registered at sea and are better represented on the eastern side of the arc due to dominant easterly winds. Dome-forming eruptions generally produce pyroclastic flows that also generally reach the sea but have limited aerial extent. Almost all eruptive episodes have significant phreatic activity which widely disperses a large amount of very fine material. This material, however, is very quickly transformed into clay during sedimentation in the sea and extremely difficult to distinguish from hemipelagic material from another origin. To reconstruct the volcanic history, the sedimentary record must not only be as complete as possible but also as least disturbed as possible by the numerous processes that may affect the submarine flanks of Lesser Antilles volcanoes: volcano flank collapses, turbidity currents generated by sediment failures on the steep submarine slopes (especially on the western coasts), and erosion by the strong deep sea currents. Due to the steep slopes of the western flanks of the volcanoes and existence of strong marine currents, the products of volcanic eruptions are rarely deposited by fallout on the sea floor without some lateral transport or reworking. In most cases, volcanic material has been reworked after initial deposition, leading to more or less blunt magmatic fragments. In addition, due to the high crystallinity of most andesitic material, glassy material is rare. Consequently, submarine sediments are considered representative of an eruptive episode if they contain volcanic material that has been only slightly modified by post-depositional transport, that is, with a significant fraction of pumice or scoria fragments that are extremely fragile and cannot be preserved over long transport distances or angular dome fragments.

Core U1397A provides a continuous record of tephra layers over the first 130 ka, with a time resolution ~2 ka. Over the top 50 m (approximately the first 110 ka), the two cores U1397A and U1397B display similar distributions of tephra layers despite significant differences in the distribution of turbidites (see **Supplementary Figure S2**), which confirms the good volcanic record at this site. Although more fragmentary, the tephra record in core 1399A allows reconstruction of the volcanic activity from

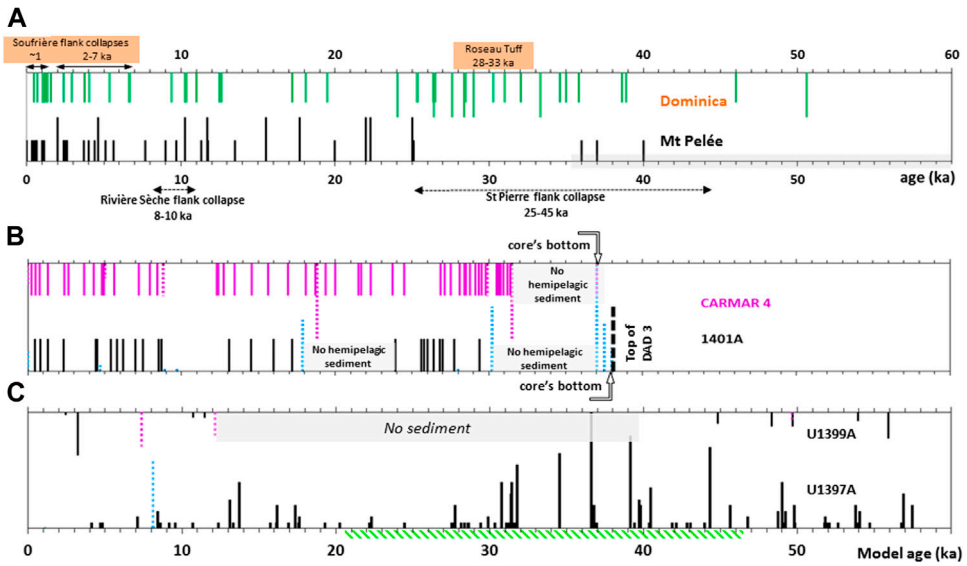


FIGURE 9 | Volcanic records on land (Mt Pelée and Dominica) and in cores U1397A, U1399A, U1401A, and CARMAR 4: 0–60 ka. **(A)** On-land dating. Data sources: 1) Dominica: flank collapses Soufrière (^{14}C; Le Friant et al., 2002), Plat Pays (K-Ar; Samper et al., 2008), and eruptions (^{14}C, Carey and Sigurdsson, 1980, Lindsay et al., 2005, Boudon et al., 2017; U-Th/He Howe et al., 2014). 2) Mt Pelée: flank collapses: "Le Prêcheur" and "St Pierre" (K-Ar, Germa et al., 2011a), "Rivière Sèche" and "St Pierre" (U-Th, Le Friant et al., 2002, Le Friant et al., 2015 and Villemant, unpublished; ^{14}C, Westercamp et al., 1989 and Boudon et al., 2013). Eruptions ages: most ^{14}C dates for Mt Pelée are relatively old measurements by bêta counting (gray zone: all ages out of ^{14}C dating range; Traineau et al., 1989); recent ^{14}C data: Michaud-Dubuy et al., 2019; others: K-Ar, Germa et al., 2011a; U-Th, Le Friant et al., 2002 and Villemant, unpublished. Age ranges of flank collapses are estimated using bracketing ages of pre- and post-flank collapse dome-forming eruptions (see also **Figure 2**). The height of the bars relates to the relative intensities of the eruptions (on-land data). **(B)** Cores U1401 A and CARMAR –4 (from Solaro et al. (2020) and Boudon et al. (2013), modified). Lines: tephra; dotted lines: turbidites (the height of the bars relates to the relative thicknesses of the turbidites). Gray domains: hemipelagic sedimentation gaps. Thick dashed line: end of core U1401A on top of the most recent DAD offshore Mt Pelée (DAD3; see **Figure 1**); its age of ~36 ka (minimum value, Solaro et al., 2020) is still questioned (see text for explanations). **(C)**: Cores U1397A and U1399A (this study). Tephra (lines) and turbidites (dotted lines) are represented with their relative thicknesses. Gray domain: sedimentation gap between 12 and 40 ka (U1399A). The green dashed domain (~20–47 ka) corresponds to the presence of large fractions of mafic scoriae in core U1397A (Del Manzo et al., in prep.). Scales are arbitrary and different for tephra layers, turbidites, and debrites.

~45 ka to ~1.5 Ma. The time resolution varies from ~4 ka for the first 450 ka to much higher values and higher uncertainties in age calibration, beyond.

In **Figure 9**, for the time period 0–60 ka, volcanic records in cores U1397A and U1399A are compared to the data of cores U1401A (Solaro et al., 2020) and CARMAR 4 (Boudon et al., 2013) and to on-land data for the eruptions of Mt Pelée and the most intense ones of South Dominica. The core U1399A does not contain significant information on that time period because of a sedimentation gap (~10–45 ka; **Figure 7A**). The site U1401A, the closest to the coast, suffers from large bias in the volcanic record because of its location in front of the flank collapse structures of Mt Pelée. Channelized pyroclastic and debris flows reaching the sea or remobilized by riverine erosion have produced the numerous turbidites recorded in this core (Solaro et al., 2020). The site CARMAR-4, close to site U1397, displays many more tephra layers than other cores during the first 5 ka likely because deposits are much less disturbed by piston coring than most other drilling techniques (**Figure 9**). The submarine cores clearly provide more complete information on the frequency of volcanic activity than on-land data that suffer from limitations in sampling and dating.

The volcanic activity in Dominica is the main activity that can interfere with Mt Pelée deposits in these cores because of its proximity and intensity. In particular, the "Roseau Tuff" eruption (28 ± 3 ka, Carey and Sigurdsson, 1980, Lindsay et al., 2005; 33.3 ± 0.4 ka Boudon et al., 2017) was the largest explosive eruption since 200 ka in the Antilles Arc (**Figure 9A**). However, the air-fall products of this eruption are mostly dispersed eastward from the Lesser Antilles Arc and almost absent on the western side of the islands (Carey and Sigurdsson, 1980). On the contrary, the voluminous pyroclastic flows of this eruption have triggered submarine pyroclastic and debris flows channelized southward to the Grenada Basin (Sparks et al., 1980a; Whitham, 1989; **Figure 1B**). Tephra layer distributions in the cores IODP340 (U1397A and U1401A) and CARMAR 4 display apparent increase in activity at that period (~25–32 ka; **Figure 9B**). Volcanic products of Dominica compared to those of other nearby islands are typically more K-rich (Carey and Sigurdsson, 1980); almost all glass compositions of tephra measured in cores U1401A (Solaro et al., 2020) and U1397A (at least over the top 50 m let ~0–130 ka, Del Manzo et al., in prep.) are typical of Mt Pelée and not of Dominica (**Figure 10A**).

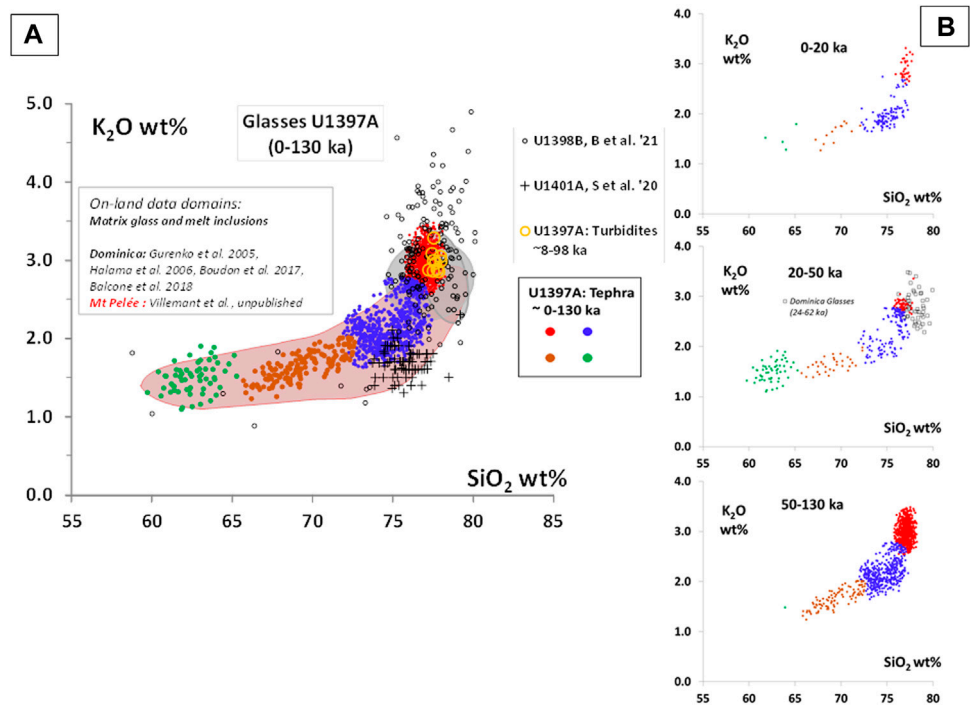


FIGURE 10 | SiO_2 and K_2O compositions of glass from cores of the IODP340 expedition. **(A)** Comparison with on-land samples of Mt Pelée and Dominica. Colored symbols: tephra (dots) and turbidites (open yellow circles) of core U1397A (top 50 m ~ 0–130 ka; Villemant et al., unpublished data and Del Manzo et al., in prep.). Tephra: the different colors correspond to arbitrary subdivisions according to the SiO_2 and K_2O concentrations. Small black circles: tephra and turbidites of core U1398B (0–900 ka, Breitkreuz et al., 2021). Black crosses: tephra and turbidites of core U1401A (0–36 ka; Solaro et al., 2020). Composition domains: matrix glass and melt inclusion compositions (on-land data). Gray domains: South Dominica (0–60 ka, Gurenko et al., 2005; Halama et al., 2006; Boudon et al., 2017; Balcone et al., 2018); red domain: Mt Pelée (0–80 ka, Villemant et al., unpublished data). **(B)** Variations in U1397A glass compositions with time. 0–20 ka: "Recent Pelée"; 20–50 ka: "Grand Rivière"; open squares: glasses from South Dominica (24–62 ka); and 50–130 ka: "Old Pelée."

In core U1397A, only few tephra glasses have Si- and K-rich glass compositions, which may correspond to Roseau Tuff eruption, and the coexistence, in the same tephra layers, of K-poor glasses that are absent in Dominica products also favor the Mt Pelée source (**Figure 10B**). In general, in these cores offshore Martinique, very few tephra deposits originate from Dominica, except in core U1398 at the front of Martinique SLDs in the Grenada Basin, which almost exclusively contains material from Dominica (Breitkreuz et al., 2021). The different types of tephra products (dome or Plinian clasts or scoriae) in cores CARMAR 4 and U1397A are not investigated in this study, but preliminary petrological data on U1397A tephra (Del Manzo et al., in prep.) indicate the presence of abundant scoriae fragments from ~50 to ~20 ka (**Figure 9C**), which is consistent with the observations in core U1401A (Solaro et al., 2020). The glass compositions of these scoriae are typical of the less Si-rich end member of "Grand Rivière" activity (**Figure 10B**).

The total number or thickness of tephra layers, averaged over different time periods (5 or 20 ka), provide estimates of the variations in sedimentation rates of magmatic products (expressed in number/ka or cm/ka; **Figure 11A**). They may also be estimated by the variations in the slopes of cumulative thickness vs. time (**Figures 8B**, **11B**). These parameters are designated under the collective term of mean deposition rate and are used as proxies of the magma production rates. These are minimum values since volcaniclastic turbidites are not included in the balance but may partly be direct products of the volcanic activity. A systematic and detailed study of the turbidites is required to evaluate their actual contribution. In addition, as discussed above, a significant part of the tephra falls (mainly from phreatic and Plinian eruptions) are not recorded in submarine deposits on the western flank of the volcano mainly due to prevailing easterly winds. For the three cores CARMAR-4, U1397A, and U1401A, the recorded activity over the common period of time of ~0–32 ka is low compared to older time periods (**Figure 11C**). In contrast to the large gaps in the tephra succession on land, particularly at > 20 ka (**Figure 9**), the volcanic activity of Mt Pelée recorded offshore is continuous from at least ~130 ka to the present day, with four main periods (**Figure 11A**).

Using cumulative tephra thickness, the most recent period (20 ka—present day) is the less active period with a mean tephra deposition rate of 3 cm/ka. This result contrasts sharply with that of previous evaluation because on-land data are typically biased by better preservation and exposure of the more recent deposits

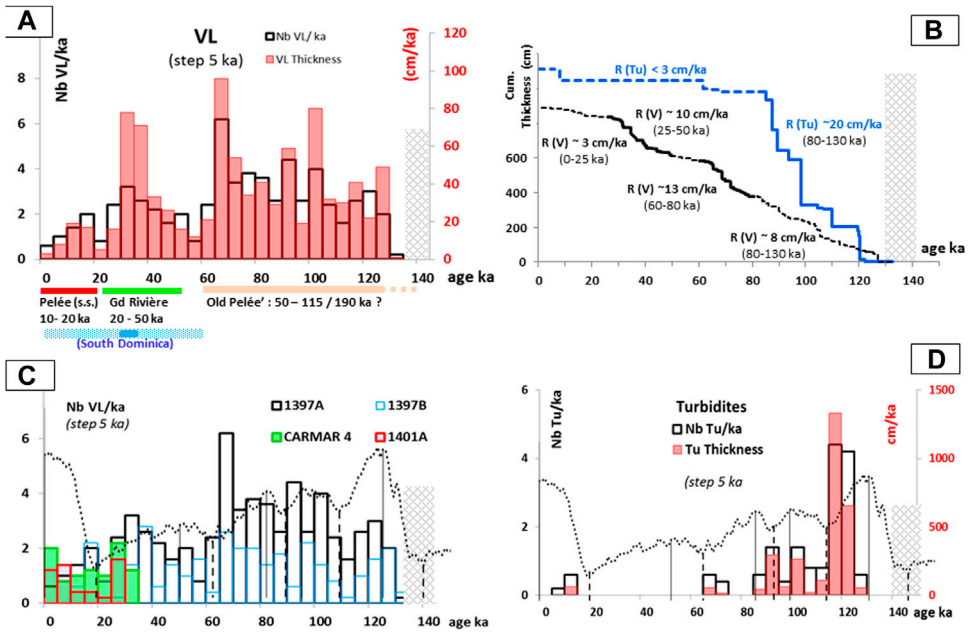


FIGURE 11 | Volcanic tephra deposition rates over the period 0–140 ka (core U1397A). **(A)** Tephra deposition rates. Nb VL/ka: total number of tephra layers (VL) per ka; VL thickness: total thickness of tephra layers per ka. Histograms are drawn with intervals of 5 ka. **(B)** Cumulative thicknesses of tephra and turbidites. R(V) and R(Tu): deposition rates of tephra and turbidites, respectively, in centimeter per ka. In brackets: intervals of time for each deposition rate estimated using a least square regression. **(C)** Comparison of tephra deposition rate estimates in cores U1397A, U1401A, and CARMAR-4. Caption as in **(A)**. Dotted lines: LR04 curves for comparison of deposition rates variations with high and lowstands of the sea level. **(D)** Deposition rates of turbidites. Caption as in **(A)**. Dashed zones: sediment gaps. Dotted lines: LR04 curves for comparison of deposition rates variations with high and lowstands of the sea level.

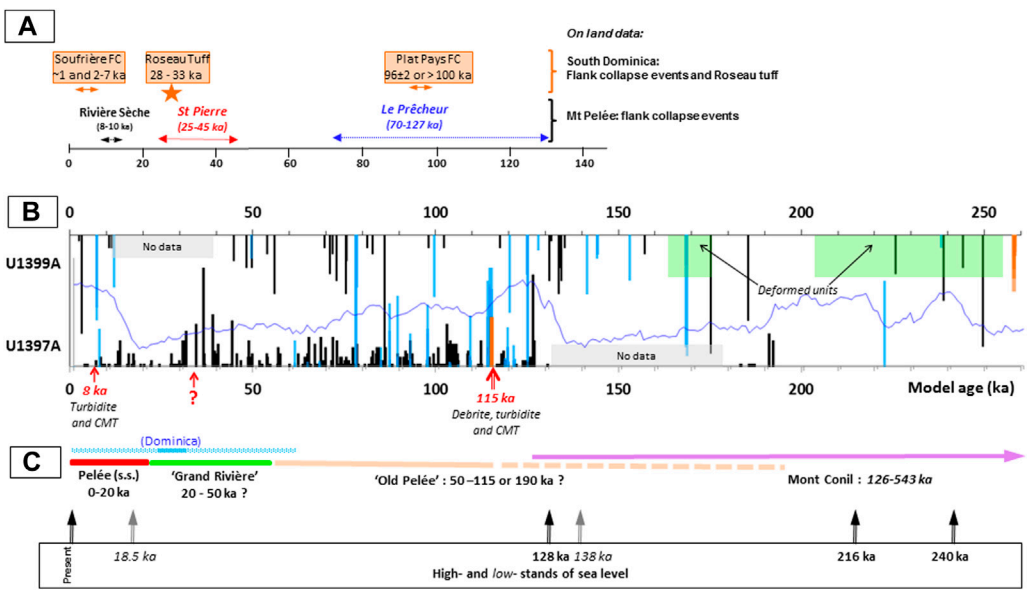


FIGURE 12 | Volcanic records on land (Mt Pelée and Dominica) and in cores U1397A and U1399A: 0–260 ka. **(A)** On-land data. **(B)** Core data. **(C)** Proposed chronology of active volcanic centers. Symbols and data sources as in **Figure 9**. Red arrows in **(B)** refer to possible flank collapses identified on land and offshore. CMT: coherent mass transport (duplicate units). Blue line: LR04 curves for comparison. Dashed lines indicate speculative extent of the volcanic activity.

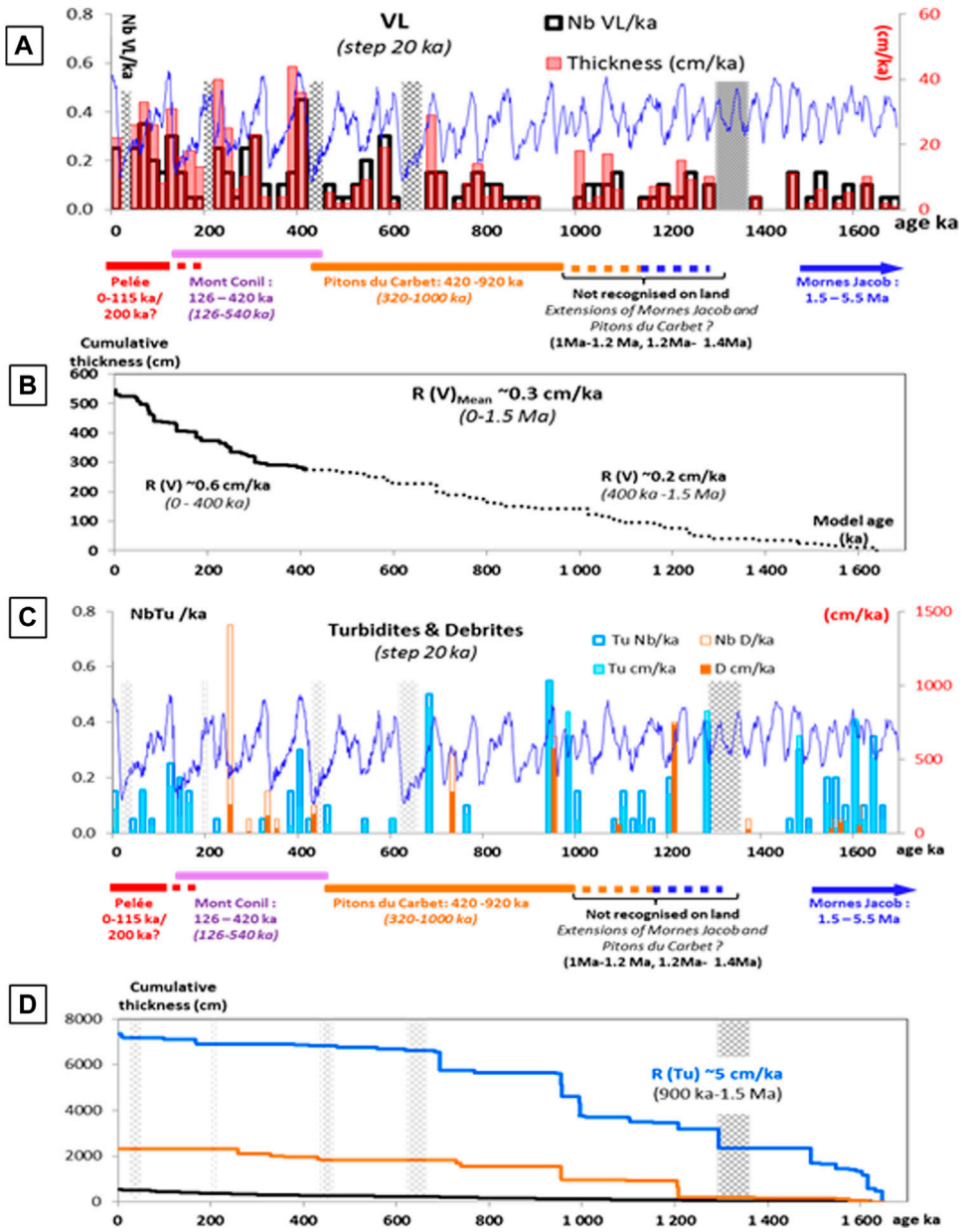


FIGURE 13 | Deposition rates of tephra and turbidites over the period 0–1.5 Ma (core U1399A). Histograms are drawn with intervals of 20 ka. Blue lines: LR04 curves for comparison of deposition rate variations with high and lowstands of the sea level. Dashed zones represent sediment lack (light gray) and void (dark gray) in the core. The height of the bars relates to the relative thicknesses of the deposits. Age ranges: this study; in brackets: previous data (K-Ar dating; Germa et al., 2010; Germa et al., 2011a). **(A)** Tephra deposition rates. Nb VL/ka: total number of tephra layers (VL) per ka; VL thickness: total thickness of tephra layers per ka. **(B)** Cumulative thicknesses of tephra. R(V): mean deposition rates of tephra in centimeter per ka. In brackets: intervals of time for each estimate. **(C)** Turbidite deposition rates. Blue bars: turbidites; orange bars: debrites. Tu Nb/ka and D Nb/ka: total number of turbidites and debrites per ka; Tu cm/ka and D cm/ka: total thickness of turbidites and debrites per ka. **(D)** Cumulative thicknesses of turbidites, debrites, and tephra. Blue line: turbidites; orange line: debrites. R(Tu): mean deposition rate of turbidites in centimeter per ka. In brackets: intervals of time for the estimate.

(see, for example, Traineau et al., 1989 and **Figure 9A**). The periods 50–20 ka and 80–50 ka have the highest mean tephra deposition rates (~10 and 13 cm/ka, respectively) with maximum activities at ~ 30 and ~70 ka, respectively (**Figure 11**). It should be emphasized that the 30–50 ka period of activity which is characterized by the emission of Grand Rivière–type magmas

is much longer and more productive than indicated by on-land investigations (Bourdier et al., 1985). In addition, the model of rejuvenation of the magmatic activity with the emission of more dense mafic magmas triggered by a major flank collapse proposed by Boudon et al. (2013) is incompatible with these new data, which provide no evidence for such triggering event at 50–60 ka, neither on land nor in the cores.

The maximum age of the last period of activity cannot be determined neither in core U1397A because of a large sediment gap (135–185 ka; **Figures 5B**, **12**) nor in core U1399A because of the low age resolution. However, the period of continuous activity lasted at least 50 ka (80–130 ka) with a tephra deposition rate roughly constant ~8 cm/ka (**Figure 11B**). All volcanic activity recorded from 130 ka is by default attributed to Mt Pelée s.l.; the petrological consistency of the whole period still requires confirmation (Del Manzo et al., in prep.).

The core U1399A provides a longer time scale (**Figure 13**). Deposition rates are minimum values since the volcanic units are under-represented in this core because of the great distance to volcanic centers and the fragmentary record. Two main activity periods are evidenced: the recent period, 0 to ~300–400 ka with a mean tephra deposition rate of ~0.6 cm/ka, and the older period (>400 ka) with a deposition rate three times lower (~0.2 cm/ka; **Figure 13B**). Over the last 130 ka, the mean tephra deposition rate at site U1399A is ~10 times lower than that at site U1397A mainly due to the greater distance to volcanic centers and the many missing sedimentary units below 50 m bsf, which lead to a significant underestimate (**Figure 6**). These results, nevertheless, indicate that the volcanic activity in Martinique was almost continuous since at least 1.5 Ma, with a few short rest periods separating several distinct activity periods that roughly correspond to those defined on land (**Figure 13A**). Three successive activity periods at North Martinique are recorded since ~1 Ma, which likely correspond to the three volcanic centers: Pitons du Carbet, Mont Conil, and finally Montagne Pelée (s.l.). In the absence of petrological arguments, it is not possible to identify the possible transition between the activities of Mt Conil and Mt Pelée (s.l.). Volcanic activity older than 1.4 Ma may correspond to that in Morne Jacob. Between 1 and 1.3 Ma, a significant volcanic activity is recorded in core U1399A but not on land. It is separated from the two other periods of activity by rest periods of ~50–100 ka (**Figure 13A**). It could correspond to an extension of the activity of either Morne Jacob or Pitons du Carbet or a still unknown activity.

5.4 Volcaniclastic Turbidites

Almost all turbidites in cores offshore Martinique are volcaniclastic turbidites. Turbidity currents can be generated by voluminous pyroclastic flows entering the sea. They can also be generated on land by remobilization by rivers of pre-existing volcaniclastic deposits (especially during cyclonic periods) or by slope failure within the sea (in that case, the volcanic material is mixed with hemipelagic sediment). The steep slopes of the western coast of Martinique and the strong marine currents favor such submarine remobilizations. The minimum age of emplacement of the turbidite (as well as debrite) is by default approximated by the age of the first overlying hemipelagic layer, but turbidite packages may have been emplaced over large intervals of time (**Figures 12**, **15**). Turbidites have highly variable thicknesses (some cm to 10 m) and are highly heterogenously distributed along the cores. They very often constitute a series of successive turbidites with total thicknesses up to 15–20 m (e.g., unit C; **Figures 4**, **6**). The abundance (or deposition rate) and distribution of turbidites directly depends on the core location. The location of site U1397A on a topographic high strongly prevents it from the influence of turbidity currents; turbidites are almost absent in the upper 30 m and scarce up to a depth of 53 m bsf (**Figures 4**, **5B**). Below, the ~17-m-thick turbidites at the base of unit C are older than 87 ka and have an average accumulation rate of ~20 cm/ka over the time interval 87–130 ka (**Figure 11B**); this suggests that this site before ~87 ka was strongly affected by turbidity currents and probably closer to the channel bed. The core U1398B located in the Grenada Basin outside the SLDs contains at its top a thick series of well-bedded turbidites of total thickness ~30 m, which represent around 2/3 of the total cored sediments (Le Friant et al., 2013). This site collects submarine sediments rich in volcaniclastic material that are remobilized by the strong turbidity currents flowing in deep channels to the Caribbean Sea. The cores U1400A and 1401A located at the outlet of the Mt Pelée collapse structures contain at their top thick turbiditic units (~25 and 50 cm, respectively) almost devoid of hemipelagic sediments (Le Friant et al., 2013); they directly collect pyroclastic material deposited on land and remobilized by rivers draining rainfall in the north of Martinique. On the contrary, core U1399A is located on SLDs, but ~70 km from the coast, contains at its top ~80 cm of hemipelagic sediments (**Figures 3**, **6**) and, in the top 60 m (Units A and B), a low proportion of turbidites with a low deposition rate (<3 cm/ka; **Figure 11B**).

Erosion of pre-existing sediments at the emplacement of turbidites is a well-documented feature (see, for example, Trofimovs et al., 2010; Trofimovs et al., 2013). The $\delta^{18}O$ chronostratigraphy in cores U1397A and U1399A indicates that erosion and/or duplication of large sedimentary units may occur at the emplacement of thick turbidite units. In core U1397A, at the base of unit C, a thick sedimentary unit comprises a sequence of turbidites that includes a 4.5-m-thick hemipelagic duplicate unit and overlays a ~1.5-m-thick series of debrites (**Figure 4**). The whole of this sedimentary unit is intercalated between two units of hemipelagic sediments separated by an interval of time of ~50 ka (**Figure 5B**). This gap is equivalent to ~14 m of hemipelagic sediment. This sediment may have been eroded by the turbidity currents that emplaced this complex sequence, or it may have slid away down slope before. On the contrary, none of the shallower and thinner turbidites in core U1397A does significantly erode pre-existing sediments. Many similar features are also observed in core U1399A below 60 m bsf; long periods of hemipelagic sedimentation (~200–430 ka, ~470–600 ka, ~780–950 ka) alternate with thick series of turbidites with large gaps in hemipelagic sedimentation that could correspond to erosion or sliding down slope at emplacement of the turbidites (**Figure 7**). In addition to low coring recovery, erosion or

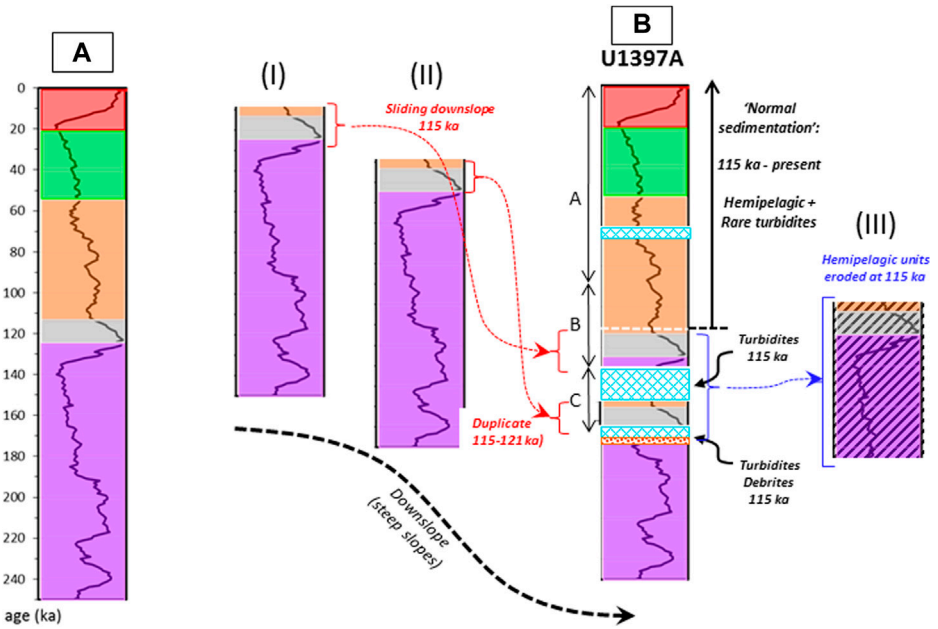


FIGURE 14 | Coherent mass transport model. **(A)** $\delta^{18}O$ stratigraphy with color codes. Black line: LR04 curve. Color codes are arbitrary (see also **Figure 15**). (I) and (II) are hypothetic logs (120–250 ka) of two sites upstream the U1397 site. Color codes from section **(A)**. **(B)** U1397A log interpretation. Color codes from section **(A)**. Dashed blue zones: turbidites. Letters are stratigraphic units defined by Le Friant et al. (2013). (III) Sediment package eroded at the emplacement of the duplicate unit and turbidites (Unit C). At ~115 ka at site U1397A, a large section of sediments deposited between 180 and 115 ka (III) was eroded, a debrite probably generated by a flank collapse, and a series of turbidites with the intercalated duplicate unit were emplaced on the remaining sediments older than 180 ka. These material slided down slope from upstream sites (I and II). Then, sedimentation continued without significant disruption since ~115 ka. This event has likely been triggered by "Le Prêcheur" flank collapse and related landslides.

duplication of hemipelagic sediment related to turbidite and debrite emplacement makes the chronostratigraphic reconstruction less robust beyond 130 ka in core U1397A and 400 ka in core U1399A.

In the absence of detailed petrological information, the origin of turbidites in cores U1397A and U1399A cannot be unambiguously established (**Figure 10**). Glass compositions of turbidites and tephra layers of core U1401A are close and clearly attributed to Mt Pelée magmas (Solaro et al., 2020; **Figure 10A**). Glass compositions of pumice clasts sampled in seven turbidites of the top 50 m of core U1397A (dated between 8 and 98 ka) have been determined. They are highly differentiated (SiO_2 ~ 77%, K_2O ~3%) and homogenous in composition, suggesting a common magma source which, however, cannot be attributed unambiguously to Mt Pelée or Dominica (**Figure 10A**). No turbidite having the same age and composition than that of Roseau Tuff eruption at ~31–33 ka in Dominica (Carey and Sigurdsson, 1980; Boudon et al., 2017) exists in cores U1397A, U1401A, and CARMAR 4 (**Figure 10B**). In core U1399A, a large sediment gap, equivalent to 12–43 ka, is due to erosion by turbidity currents and/or submarine landslides and cannot be solely related to the Roseau Tuff event (**Figure 7A**).

The temporal distribution of the accumulation rates of turbidites offshore Martinique is generally not in phase with the accumulation rates of tephra layers (**Figures 11B**, **13C**). Most eruptions are of low intensity (much less than the exceptional eruption of Roseau Tuff, for example) and pyroclastic flows spread weakly or even do not reach the sea. Most volcaniclastic turbidites are likely the result of the remobilization of pyroclastic deposits on land and on the sea floor, rather than direct deposits of pyroclastic falls or flows. Reid et al. (1996) have suggested that in the back-arc region of the Antilles during low stands of the sea level, volcanic turbidites are thicker and/or more frequent because of the increase of inter-island currents and of erosion of insular shelves. Our results show that it is not the case offshore Martinique and that turbidites are more frequent close to high-stand periods (**Figures 11D**, **13C**). They are not primarily triggered by the variations in sea water level, but highstands naturally increase the probability for pyroclastic falls and flows to reach the sea or for on-land pyroclastic deposits to be transported to the sea by rivers.

5.5 Submarine Landslides: Duplicate Units, Debrites, and Deformed Deposits

The reconstructed chronostratigraphy of cores U1397A and U1399A highlight two main types of sliding of submarine sediments. The first one is a coherent mass transport mainly driven by gravitational failure of steep slope and the second one corresponds to thrusting at the front of large submarine landslides on relatively flat slopes and induces sediment deformation. The first type is favored by the steep slopes of

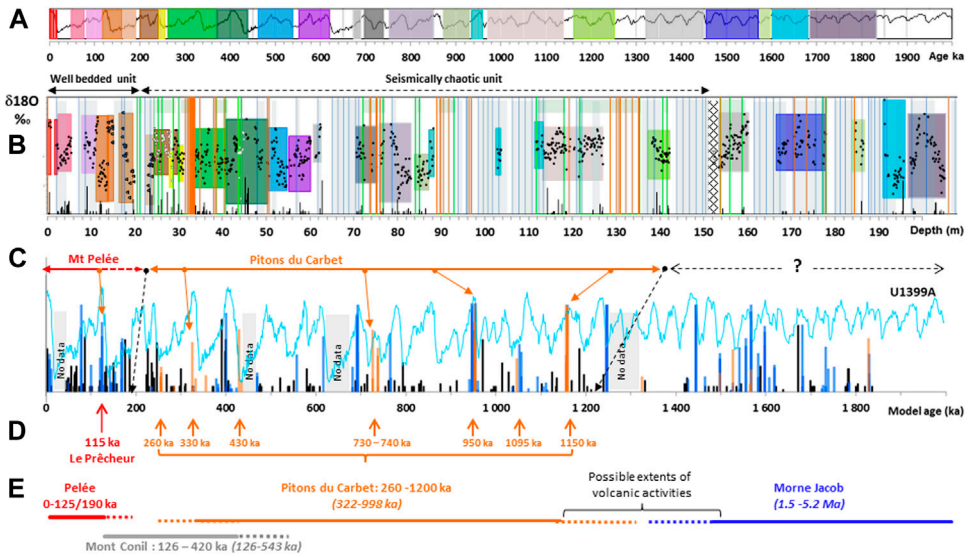


FIGURE 15 | Chronological model of the evolution of volcanic activity in Martinique over the last 1.5 Ma. (The reader is referred to high-resolution figure on the web version of this article for benefit). **(A)** LR04 reference curve for $\delta^{18}O$ evolution of seawater. Color codes are arbitrary and used for comparison with U1399A stratigraphy **(B)**. **(B)** Stratigraphy and $\delta^{18}O$ of hemipelagic sediments of core U1399A. Colored domains correspond to different hemipelagic units characterized by their $\delta^{18}O$ patterns and their age range as defined in **(A)**. Other symbols as in **Figure 6**. **(C)** Reconstituted chronostratigraphy of volcanic events recorded in core U1399A. Symbols as in **Figures 6**, **7C**. Blue line: LR04 curve (unscaled) for comparison of volcanic activity (tephra, turbidites, and debrites) with high and lowstands of the sea level. Orange arrows: main flank collapses identified by debrites and/or turbidites. Black arrows: main rest periods delimiting volcanic activities of Mt Pelée and Pitons du Carbet. **(D)** Scenario of the main flank collapses. Arrows: main flank collapses. **(E)** New model for the volcanic activities of Mt Pelée and Pitons du Carbet. Age ranges in brackets: previous data (K-Ar dating; Germa et al., 2010; Germa et al., 2011b). Mt Pelée activity and "Le Prêcheur" flank collapse are dated from the core U1397A (**Figure 12**). Mt Conil and Morne Jacob activities are not well-constrained by our data.

the volcano close to the shore (as for sites U1397A and U1401A, **Figure 1B**), where sliding is triggered by slope failure and gravity and preserves thick coherent sedimentary units, with no significant internal deformation. Triggering events are various as, for example, high-energy pyroclastic flow entering the sea, debris avalanches generated by flank collapses, intensification of submarine currents during glacial low stands, or high-magnitude earthquakes. On relatively flat slopes at a distance from the shore (as for site U1399A, **Figure 1B**), sliding of very thick sedimentary units implies a significantly different transport mechanism, with deformation of the displaced units.

Such type of behaviors have been proposed by numerous authors for emplacement of SLDs (see, for example., Frey-Martínez et al., 2006; Watt et al., 2012; Le Friant et al., 2015; Brunet et al., 2016; Le Friant et al., 2020); the entrance of debris avalanches in the sea generates debrites and turbidites. It may also generate slope failure and coherent mass transport ('duplicate units') or erosion of pre-existing sediment, especially on steep slopes near the shore. If the accumulated load is large enough, it can induce or reactivate submarine landslides with failure, deformation, and transport of the pre-existing sedimentary units at long distances from the origin (Lafuerza et al., 2014; Hornbach et al., 2015; Le Friant et al., 2020).

The hemipelagic sediments of the top 28 m of core U1397A (unit A) display a continuous $\delta^{18}O$ pattern consistent with the time period 0–87 ka (**Figures 4**, **5B**). Numerous turbidites are intercalated in hemipelagic sediments of unit B (28–53 m bsf; **Figure 4**), but the reconstructed $\delta^{18}O$ pattern is continuous and consistent with the time period 87–132 ka (**Figure 5B**). Unit C (53–76 m bsf) is a complex sequence of turbidites and debrites containing a ~4.5-m-thick unit of hemipelagic sediments which display a $\delta^{18}O$ pattern consistent with the time period 115–121 ka (**Figures 4**, **5B**). We interpret these features as the result of coherent mass transport of pre-existing sediments triggered by a major flank collapse of Mt Pelée at ~115 ka (**Figure 14**). The debris avalanches that entered the sea strongly eroded pre-existing sediments and deposited the debrite units. This event produced large volcaniclastic turbidites possibly containing an eruptive component synchronous of the flank collapse. Simultaneously, the rapid sediment overloading triggered submarine slope failures and coherent mass transports of pre-existing sediments (deposited between 121 and 115 ka) down the slope rather than simply eroding these slope sediments (**Figure 14**). These events were followed by a period of numerous volcaniclastic turbidity currents (between 115 and 87 ka). Thereafter, no other more recent process significantly disturbed the sedimentation at the site U1397A.

The 115 ka event is also recorded in site U1399A at the base of the upper well-bedded seismic facies (**Figure 3B**). At the base of

unit A (14–23 m bsf), a series of three duplicate hemipelagic units is intercalated within turbidites (**Figure 6A**). They represent the sedimentation time interval 115–150 ka (**Figure 7C**). These units likely slided as coherent mass transports simultaneously with a massive turbidite. Debris flows cannot be transported over long distances in the sea, which explains the absence of the debrite at that time in core U1399A. On the contrary, the stress generated by the overload may have propagated over long distances in pre-exiting sediments and activated (or re-activated) sliding and deformation in the thick deformed units existing below unit A (**Figure 6A**). Contrary to shallower well-bedded sediments (cores U1397A, U1401A, and unit A of core U1399A), thick discrete units below 23 m bsf in core U1399A are strongly deformed (**Figure 6A**). They are considered possible zones of décollement favoring landsliding (Lafuerza et al., 2014; Hornbach et al., 2015; Le Friant et al., 2020). These décollement and deformation zones may be reactivated at different periods by successive flank collapses that are necessarily older than the undeformed sediments of the overlying well-bedded unit, that is, older than 150 ka (**Figures 3B**, **13**).

Coherent mass transport processes are likely the cause of the anomalous $\delta^{18}O$ patterns in hemipelagic sediment units at ~4–5 m and ~6–8 m bsf in core U1401A, associated with turbidites (Solaro et al., 2020; **Figure 5B**); they rather correspond to duplicate units. To reconcile their $\delta^{18}O$ patterns with standard reference curves, flank failure should have occurred at 8 and 14 ka. In core U1397A, the youngest turbidite is ~8 ka old (**Figure 5B**), which suggests a common origin of the three events. Because site U1401A is located at the outlet of the Mt Pelée collapse basin, it has better chance to record less intense (and most recent) events than the more distant sites (U1397A and U1399A). This interpretation supports the hypothesis of the existence of a low-magnitude flank collapse at ~8 ka ("Rivière Sèche" flank collapse, Le Friant et al., 2002).

In core U1399A, at least four duplicate units can be identified between ~23 and 45 m bsf in the upper part of the SLDs (**Figures 3B**, **6A**, Le Friant et al., 2015). Their thickness varies from ~1.5 to ~10 m, and they are generally closely associated with turbidites and deformed intervals (**Figures 6A**, **7C**). The maximum ages of transport of these units are 115–150 ka and 210, 220 and 375 ka. Other duplicate units may exist at greater depth, but the low resolution and the sediment gaps prevent any identification. Several debrites are identified inside the landslide (~23–150 m bsf, units B to F), dated at 260, 290, 325–330, 430–440, 730–740, 950, 1,100, and 1,150 ka (**Figure 7C**). Most debrites are closely associated with thick turbidites, which suggests that they correspond to distal deposits of large debris flows (Talling et al., 2010). Finally, the debrite deposits at 430 ka overlay a large sediment gap of ~1.5 m hemipelagic sediments, which is likely an erosive gap. All these features may represent tracers of large flank collapses that occurred between 260 and 1,150 ka and strongly disturbed the sedimentation.

Below ~150 m bsf in the core U1399A, in the seismic well-bedded facies (units G and H), the sediments consist of a succession of thick turbidite sequences (up to 25 m thick) including 5–10 m thick hemipelagic sediment units and some debrite deposits dated at 1.5–1.55 Ma and ~1.8 Ma (confidence upper limit of dating), which could also be the result of large flank collapses.

6 CHRONOLOGY OF THE VOLCANIC ACTIVITY IN MARTINIQUE SINCE 1.5 MA

The reconstructed chronology of volcanic eruptions and flank collapses recorded in cores U1397A and U1399A are summarized in **Figures 12**, **15** (0–1.5 Ma).

6.1 Mt Pelée

6.1.1 Flank Collapses

The major event identified in both cores is dated at 115 ka (**Figure 12**). It corresponds to the "Le Prêcheur" flank collapse of Mt Pelée dated on land between 70 and 127 ka (Le Friant et al., 2003; Germa et al., 2011a; **Figure 2B**). It is the largest flank collapse that affected the Mt Pelée volcano. Its impact on submarine sediments spread over a large sector and at a great distance: ~70 km on-axis of the collapse structure (site U1399A) and at least 30 km off-axis (site U1397A; **Figure 1B**). It represents a much larger area than that defined by the blocky unit (DAD3) and the extent of topographic scarps identified offshore Martinique (Le Friant et al., 2003; Le Friant et al., 2015; **Figure 1B**). However, another interpretation must consider the Plat Pays flank collapse south of Dominica which is at least ~100 ka old (Le Friant et al., 2002; Samper et al., 2008). The estimates of collapse volumes on land (~20–25 km^3) and volumes of chaotic deposits offshore (~250 km^3) are similar for Plat Pays and "Le Prêcheur" events (Le Friant et al., 2002; Le Friant et al., 2003). In addition, distances of both collapse structures to site U1397A are similar (**Figure 1B**). Since the site U1397A is located south of the deep (>3,000 m) submarine channel between Dominica and Martinique, it is likely that most debris flows and submarine landslides originating from Dominica have been channeled toward the Grenada Basin and did not affect the western flank of Martinique.

The existence of two younger flank collapses at Mt Pelée ("St Pierre" and "Rivière Sèche"; Le Friant et al., 2003; Germa et al., 2011a; **Figure 2B**) is still questioned as they are not recorded as specific deposits in both cores (**Figure 9**). Coherent mass transports in core U1401A are contemporaneous of a thick turbidite in core U1397A dated at ~8 ka that could correspond to a low-magnitude flank collapse (**Figure 5B**). The "Rivière Sèche" structure, previously dated at 8–10 ka, was related to the debris avalanche deposit DAD 3 because the missing volume on land and the DAD 3 volume are similar (Le Friant et al., 2003; **Figures 2**, **12**). However, the sediments cored at site U1401A above the DAD 3 are older than 36 ka (Solaro et al., 2020; **Figure 1B**). The DAD 3 could, therefore, result from the "St Pierre" flank collapse structure dated on land at 30–45 ka (Le Friant et al., 2003; **Figure 2**), but the estimated collapse volume is much larger than that of the deposit. Thus, the attribution of DAD 3 to a collapse structure on land remains

an open question: if the DAD 3 is related to the "Rivière Sèche" event and dated older than 36 ka as suggested by Solaro et al. (2020); a younger not yet identified flank collapse occurred at ~8 ka. However, since the U1401A core contains numerous turbidites and likely two duplicate units (see §V-5; **Figure 5B**), we suggest that some of these sedimentary units could have slided over the DAD 3 after its emplacement leading to an erroneous estimate of its actual age.

6.1.2 Volcanic Activity

Three main activity periods are identified at Mt Pelée. Their approximate age limits are "Old Pelée" > 127 ka to 50 ka; the "Grand Rivière" 50–20 ka; and "Recent Pelée" 20 ka to the present day (**Figure 12B**). The "Grand Rivière" and "Old Pelée" activity periods are much more intense than estimated in previous studies on land, and the volcanic activity of Mt Pelée strongly decreased since the last 30 ka. The "Grand Rivière" activity culminates at ~30 ka and is characterized by the emission of scoriae of mafic andesite compositions that were only emitted as enclaves during the other periods (Boudon et al., 2013). The onset of Mt Pelée activity cannot be clearly identified. The first edifice of Mt Pelée, which was at least as large as the present edifice, partially collapsed during the "Le Prêcheur" event at 115 ka, and one can imagine that a time interval of the same order of magnitude was necessary for its construction. Because the tephra records indicate more or less continuous volcanic activity on Martinique since ~190 ka, preceded by a rest period of ~30 ka, we suggest that Mt Pelée activity could have started at ~190 ka (**Figure 12**). On the other hand, the Mt Conil volcano north of Mt Pelée was active between 543 and 126 ka (Germa et al., 2011b), and a partial overlap of the activities of the two edifices must be considered (**Figure 12**). Only detailed petrological investigations are able to resolve this ambiguity.

6.2 Pitons Du Carbet

The submarine landslide units (s.s.) identified from seismic reflexion profiles and core descriptions (Le Friant et al., 2015; Brunet et al., 2016; Le Friant et al., 2020; **Figure 3B**) in core U1399A are covered by well-bedded and undeformed sediments (upper 25 m) younger than ~150 ka. Since that time, there has been no evidence in this core that large submarine landslides were able to displace and deform pre-existing sediments at long distances (>70 km) offshore Martinique. The sediments below 25 m bsf in core U1399A consist of a complex association of debrites, turbidites, and hemipelagic units. The characteristics of these complex sedimentary features are similar to those of the younger deposits related to "Le Prêcheur" flank collapse, except that turbidites are significantly thicker. We propose that they are also the result of high-magnitude flank collapses that produced, transported, or deformed sediments at distances as large as ~70 km from the Martinique shore. Their ages (between 260 and 1,160 ka; **Figure 15**) suggest that they originate from the Pitons du Carbet volcano that was active at least between 322 and 998 ka (Samper et al., 2008; Germa et al., 2011b) and experienced the largest flank collapses of all Lesser Antilles volcanoes (Boudon et al., 2007; Boudon et al., 2013; **Figure 2A**). The topographic scarps identified on submarine topography show that submarine landslides cover a large sector including the outlets of Mt Pelée and Pitons du Carbet collapse basins (**Figure 1B**). Compared to Mt Pelée activity, the tephra deposition rate of Pitons du Carbet eruptions recorded in core U1399A is significantly lower (**Figure 12**). This difference is likely due to the fact that most eruptions produced rhyodacitic lava domes with low dispersion of eruptive products.

7 SUMMARY AND CONCLUSION

The core U1397A provides the longest continuous record offshore Martinique of the hemipelagic sedimentation and volcanic explosive activity over the last 130 ka. The sedimentation along the north western flank of Martinique is dominated by hemipelagic sediments with numerous thin tephra deposits that record the volcanic activity of the volcanic island. The hemipelagic sedimentation is mainly controlled by inputs of the strong marine currents and the volcaniclastic terrigenous sediments. It rapidly decreases with distance from the island, typically from ~30 cm/ka at the shore to 5 cm/ka at 70 km from the shore. In cores U1397 and U1399 to U1401 offshore Martinique, only Mt Pelée activity was recorded in the last 150 ka. Older sediments likely record the activity of Pitons du Carbet. The absence of volcanic deposits from nearby islands, especially Dominica, is explained by the fact that the products of the most explosive phases (Plinian) were mainly dispersed to the east of the islands (due to dominant winds), while the pyroclastic flows entering the Caribbean Sea were channeled westward. The reconstituted tephrostratigraphy indicates more intense and longer activity periods than recorded on land. The volcanic history of Mt Pelée before 20 ka is significantly revised. This activity started ~190 ka ago and strongly decreased since 20 ka ("Recent Pelée" activity). The main activity period between 20 and 50 ka called 'Grand Rivière' is characterized by the emission of large amounts of mafic andesites contrary to other periods which are dominated by silicic andesites. The volcanic history older than 200 ka is less accurately recorded offshore Martinique. The significant volcanic activity recorded between 260 and 1,200 ka likely corresponds to the whole Pitons du Carbet activity. During that period, the volcanic activity recorded offshore Martinique is, however, much less intense than that of Mt Pelée recorded in the more recent deposits.

The hemipelagic and volcanic tephra sedimentation records offshore Martinique are strongly disturbed by numerous instabilities of the sedimentary piles induced by several flank collapses of Mt Pelée and Pitons du Carbet volcanoes. These events produced different deposits and instabilities in sea floor sediments. They were almost systematically accompanied by volcaniclastic turbidity currents and produced debris avalanches of limited extent

in the sea that are only represented in the most proximal cores in front of the collapse structures (cores U1400 and U1401) but could not be penetrated by drilling. Remobilization of these material produced finer deposits (debrites) observed in the cores. Loading of large amounts of collapse material at the slope break probably induced slope failures of the sea floor sediments with small-scale coherent mass transports over relatively limited distances and large-scale sediment failures with generally multiphase episodes of sliding and deformation. These features can be identified in the cores as duplicate layers and deformed sediment intervals. The reconstructed chronostratigraphy facilitates dating the major flank collapses that affected Mt Pelée and Pitons du Carbet volcanoes. The best documented event is the Le Prêcheur event dated at 115 ka, which is the last major flank collapse of Mt Pelée, which has affected the sea floor sediments up to 80 km from the coast. The younger "St Pierre" flank collapse is not clearly evidenced in the studied cores, and its dating is still uncertain. Finally, traces of a 8 ka old, low-amplitude flank collapse ("Rivière Sèche") are found in proximal cores (U1401 and U1397) and could have produced the DAD 3. Pitons du Carbet volcano is characterized by numerous large flank collapses (around 1 every 100 ka over ~1 Ma).

Holes drilled southeast of Montserrat during the IODP 340 expedition show that flank collapses (130 ka and younger) there occurred toward the end of periods of relatively elevated volcanism, and their timing also seemed to coincide with periods of rapid sea level rise (Coussens et al., 2016a; Coussens et al., 2016b). Our data offshore Martinique, however, do not show a clear relationship between the occurrence of flank collapses and the sea level variations, except that they seem to occur more frequent close to sea level highstands (as do emplacements of volcaniclastic turbidites). There is also no evidence for a relationship between the emission of more mafic magmas during "Grand Rivière" activity and a large flank collapse, contrary to previous hypotheses based on the few available data on land (Boudon et al., 2013).

The reconstructed chronostratigraphy of cores U1397 and U1399 constitutes the framework to establish the volcanic history of the volcanoes of the north of Martinique since 1.5 Ma and study the processes that may control the shallow evolution of the volcanic edifices and their instabilities. The detailed study of the petrology of the tephra layers and volcaniclastic turbidites, and of the emplacement and deformation processes within the SLDs, constitute the main methods of investigation using core material, which can be developed from this study.

DATA AVAILABILITY STATEMENT

The original contributions presented in the study are included in the article/**Supplementary Material**; further inquiries can be directed to the corresponding author.

AUTHOR CONTRIBUTIONS

All authors equally contributed to data acquisition. BV and AF were the main contributors to data interpretation and manuscript redaction.

FUNDING

This study was supported by the ANR-13-BS06-0009 CARIB, the Labex UnivEarthS, and by the PREST project co-funded by Interreg Caraibes for the European Regional Development Fund.

ACKNOWLEDGMENTS

We thank the captains, officers, and crews of the R/V JOIDES Resolution and the IODP 340 scientists. Authors are indebted to two reviewers for their detailed and constructive reviews.

SUPPLEMENTARY MATERIAL

The Supplementary Material for this article can be found online at: https://www.frontiersin.org/articles/10.3389/feart.2022.767485/full#supplementary-material

Supplementary Figure 1 | High-resolution stratigraphic logs of cores U1397A and U1399A. Black: tephra; blue: turbidite; orange: debrite. Height of black lines corresponds to the relative thickness of tephra deposits. Only main turbidites are reported as dark blue lines. Light blue zones correspond to the accumulation of numerous thin turbidites. Letters: lithological units defined on board (Le Friant et al., 2013). See also **Figure 3**. The reader is referred to the web version of this article for benefit.

Supplementary Figure 2 | Comparison of tephra layers and turbidite records in cores U1397A and U1397B. Black: tephra; blue: turbidite; orange: debrite. Height corresponds to their relative thickness of tephra layers. Scales are different for each deposit type. **(A)** Distribution as a function of the depth in core (cm). **(B)** Distribution as a function of the model age (in ka). It is to be noted that the same model age (sediments thickness vs. age) has been used for both cores with an additional shift of 9 ka for core U1397B.

Supplementary Figure 3 | Calibration of $\delta^{18}O$—age curves. **(A)** Well-calibrated curves at CARMON-2 site (blue line) offshore Montserrat (Le Friant et al., 2008), ODP999 (light blue line), and VM78-122 (purple line) in the western and eastern Caribbean Sea (Broecker W. et al., 1988; Broecker W. S. et al., 1988; Broecker et al., 1990) are used to calculate a "mean Caribbean" curve over the last 200 ka. The SPECMAP LR-04 reference curve (green line; Liesecki and Raymo, 2005) is used for ages older than 200 ka. **(B)** Reconstructed (best fit) $\delta^{18}O$ age curve for cores U1397A (red dots) and U1399A (black dots) over 0–130 ka. See the text for method description. Open red circles: CARMAR-4 curve (Boudon et al., 2013; Solaro et al., 2020). Age uncertainties are estimated ~2 ka for U1397A and ~5 ka for U1399B over this age range. **(C)** Residues of fits (measured δ18O- calculated δ18O from 'mean Caribbean' curve) for cores U1397A (red dots) and U1398A (black dots) and CARMAR-4 (open circles). Error bars: reproducibility (±1 sigma; two to four determinations per sample) on δ18O measurements in core U1397A. All residues are within ±0.5‰ and within analytical reproducibility.

Supplementary Table 1 | $\delta^{18}O$ data. Depth in core, cumulative hemipelagic sediment thicknesses, $\delta^{18}O$ data, and model ages. **(A)** U1397A. **(B)** U1399A.

Supplementary Table 2 | ^{14}C dating of foraminifers from cores U1397A and U1399A. **(A)** U1397A. **(B)** U1399A. Calibrations from Stuiver and Reimer (1993), Reimer et al. (2013a), Reimer et al. (2013b). Dataset marine 13; ^{14}C Delta R (mean): –27 ± 11 (CALIB Rev 7.0.4 radiocarbon calibration program 1986–2017).

Supplementary Table 3 | Chronology of the volcanic activity and flank collapses at Mt Pelée. Eruptive Style: dome: lava dome; BAF: block and ash flow; Plinian: plinian fall or flow; scoriae: scoria fall or flow; *: major eruption; FC: flank collapse. For sake of simplification, all ages are given in ka (kilo annum) whatever the dating technique; for source data and uncertainties, the reader is referred to references. Data sources: 1) Germa et al. (2011a); 2) Le Friant et al. (2002); 3) U-Th Villemant, unpublished data; 4) Westercamp et al. (1989); 5) Michaud-Dubuy (2019), 6) Ishizuka et al., unpublished data.

REFERENCES

Annen, C., Pichavant, M., Bachmann, O., and Burgisser, A. (2008). Conditions for the Growth of a Long-Lived Shallow Crustal Magma Chamber below Mount Pelee Volcano (Martinique, Lesser Antilles Arc). *J. Geophys. Res.* 113, b07209. doi:10.1029/2007jb005049

Balcone-Boissard, H., Boudon, G., Blundy, J. D., Martel, C., Brooker, R. A., Deloule, E., Solaro, C., and Matjuschkin, V. (2018). Deep Pre-Eruptive Storage of Silicic Magmas Feeding Plinian and Dome-Forming Eruptions of Central and Northern Dominica (Lesser Antilles) Inferred From Volatile Contents of Melt Inclusions. *Contrib. Mineral. Petrol.* 173, 101. doi:10.1007/s00410-018-1528-4

Boudon, G., Balcone-Boissard, H., Solaro, C., and Martel, C. (2017). Revised Chronostratigraphy of Recurrent Ignimbritic Eruptions in Dominica (Lesser Antilles Arc): Implications on the Behavior of the Magma Plumbing System. *J. Volcanology Geothermal Res.* 343, 135–154. doi:10.1016/j.jvolgeores.2017.06.022

Boudon, G., Le Friant, A., Komorowski, J.-C., Deplus, C., and Semet, M. P. (2007). Volcano Flank Instability in the Lesser Antilles Arc: Diversity of Scale, Processes, and Temporal Recurrence. *J. Geophys. Res.* 112, B08205. doi:10.1029/2006JB004674

Boudon, G., Le Friant, A., Villemant, B., and Viodé, J.-P. (2005). "Martinique," in *Volcanic hazard Atlas of the Lesser Antilles*. Editors J. M. Lindsay, R. E. A. Robertson, J. B. Shepherd, and S. Ali (Trinidad and Tobago, West Indies: Seismic Research Unit, The University of the West Indies), 65–102.

Boudon, G., Villemant, B., Friant, A. L., Paterne, M., and Cortijo, E. (2013). Role of Large Flank-Collapse Events on Magma Evolution of Volcanoes. Insights from the Lesser Antilles Arc. *J. Volcanology Geothermal Res.* 263, 224–237. doi:10.1016/j.jvolgeores.2013.03.009

Bourdier, J. L., Gourgaud, A., and Vincent, P. M. (1985). Magma Mixing in a Main Stage of Formation of Montagne Pelée: the Saint Vincent-type Scoria Flow Sequence (Martinique, F.W.I.). *J. Volcanology Geothermal Res.* 25, 309–332. doi:10.1016/0377-0273(85)90019-8

Bouysse, P., Westercamp, D., and Andreieff, P. (1990). The Lesser Antilles Island Arc. *Proc. Ocean Drilling Program B: Scientific Results* 110, 29–44. doi:10.2973/odp.proc.sr.110.166.1990

Breitkreuz, C., Schmitt, A. K., Repstock, A., Krause, J., Schulz, B., Bergmann, F., et al. (2021). Record and Provenance of Pleistocene Volcaniclastic Turbidites from the central Lesser Antilles (IODP Expedition 340, Site U1398B). *Mar. Geology.* 438, 106536. doi:10.1016/j.margeo.2021.106536

Broecker, W., Klas, M., Ragano-Beavan, N., Mathieu, G., Mix, A., Andree, M., et al. (1988). Introduction. *Radiocarbon* 30, 261–263. doi:10.1017/s0033822200044234

Broecker, W. S., Andree, M., Bonani, G., Wolfli, W., Klas, M., Mix, A., et al. (1988). Comparison between Radiocarbon Ages Obtained on Coexisting Planktonic Foraminifera. *Paleoceanography* 3, 647–657. doi:10.1029/PA003i006p00647

Broecker, W. S., Klas, M., Clark, E., Trumbore, S., Bonani, G., Wölfli, W., et al. (1990). Accelerator Mass Spectrometric Radiocarbon Measurements on Foraminifera Shells from Deep-Sea Cores. *Radiocarbon* 32, 119–133. doi:10.1017/s003382220004011x

Brunet, M., Le Friant, A., Boudon, G., Lafuerza, S., Talling, P., Hornbach, M., et al. (2016). Composition, Geometry, and Emplacement Dynamics of a Large Volcanic Island Landslide Offshore Martinique: From Volcano Flank-Collapse to Seafloor Sediment Failure? *Geochem. Geophys. Geosyst.* 17 (3), 699–724. doi:10.1002/2015GC006034

Brunet, M., Moretti, L., Le Friant, A., Mangeney, A., and Fernandez Nieto, E. (2017). Numerical Simulations of 30-45 Ka Debris Avalanche Flow of Montagne Pelee Volcano, Martinique: from Volcano Flank-Collapse to Submarine Emplacement. *Nat. Hazards* 87 (I2), p1189–1222. doi:10.1007/s11069-017-2815-5

Carazzo, G., Tait, S., Kaminski, E., and Gardner, J. E. (2012). The Recent Plinian Explosive Activity of Mt. Pelée Volcano (Lesser Antilles): The P1 AD 1300 Eruption. *Bull. Volcanol* 74, 2187–2203. doi:10.1007/s00445-012-0655-4

Carey, S. N., and Sigurdsson, H. (1980). The Roseau Ash: Deep-Sea Tephra Deposits from a Major Eruption on Dominica, Lesser Antilles Arc. *J. Volcanology Geothermal Res.* 7, 67–86. doi:10.1016/0377-0273(80)90020-7

Carey, S. (1999). "Volcaniclastic Sedimentation Around Island Arcs," in *Encyclopedia of Volcanoes. Part IV. Explosive Volcanism*. Editors H. Sigurdsson, B. Houghton, S. McNutt, H. Rymer, and J. Stix (New York: Academic Press), 627–642.

Cassidy, M., Watt, S. F. L., Palmer, M. R., Trofimovs, J., Symons, W., Maclachlan, S. E., et al. (2014). Construction of Volcanic Records from marine Sediment Cores: A Review and Case Study (Montserrat, West Indies). *Earth-Science Rev.* 138, 137–155. doi:10.1016/j.earscirev.2014.08.008

Clark, P. U., Archer, D., Pollard, D., Blum, J. D., Rial, J. A., Brovkin, V., et al. (2006). The Middle Pleistocene Transition: Characteristics, Mechanisms, and Implications for Long-Term Changes in Atmospheric pCO2. *Quat. Sci. Rev.* 25, 3150–3184. doi:10.1016/j.quascirev.2006.07.008

Coussens, M. F., Wall-Palmer, D., Talling, P. J., Watt, S. F. L., Hatter, S. J., Cassidy, M., et al. (2016a). "Synthesis: Stratigraphy and Age Control for IODP Sites U1394, U1395, and U1396 Offshore Montserrat in the Lesser Antilles," in *Proceedings of the Integrated Ocean Drilling Program, Principal Investigators*. Editors A. Le Friant, O. Ishizuka, and N. A. Stroncik (College Station, Tex: Ocean Drill. Program), 340. doi:10.2204/iodp.proc.340.204.2016

Coussens, M. F., Wall-Palmer, D., Talling, P. J., Watt, S. F. L., Cassidy, M., Jutzeler, M., et al. (2016b). The Relationship between Eruptive Activity, Flank Collapse, and Sea Level at Volcanic Islands: A Long-Term (>1 Ma) Record Offshore Montserrat, Lesser Antilles. *Geochem. Geophys. Geosyst.* 17, 2591–2611. doi:10.1002/2015GC006053

Deplus, C., Le Friant, A., Boudon, G., Komorowski, J.-C., Villemant, B., Harford, C., et al. (2001). Submarine Evidence for Large-Scale Debris Avalanches in the Lesser Antilles Arc. *Earth Planet. Sci. Lett.* 192, 145–157. doi:10.1016/s0012-821x(01)00444-7

Feuillet, N., Manighetti, I., Tapponnier, P., and Jacques, E. (2002). Arc Parallel Extension and Localization of Volcanic Complexes in Guadeloupe, Lesser Antilles. *J. Geophys. Res.* 107, ETG 3-1–ETG 3-29. doi:10.1029/2001JB000308

Fichaut, M., Maury, R. C., Traineau, H., Westercamp, D., Joron, J.-L., Gourgaud, A., et al. (1989). Magmatology of Mt Pele´e (Martinique, F.W.I), III, Fractional crystallisation versus magma mixing. *J. Volcanol. Geotherm. Res.* 38 (1– 2), 189–213. doi:10.1016/0377-0273(89)90037-1

Fraass, A. J., Wall-Palmer, D., Leckie, R. M., Hatfield, R. G., Burns, S. J., Le Friant, A., et al. (2017). A Revised Plio-Pleistocene Age Model and Paleoceanography of the Northeastern Caribbean Sea: IODP Site U1396 off Montserrat, Lesser Antilles. *Stratigraphy* 13, 183–203. doi:10.29041/strat.13.3.183-203

Frey-Martínez, J., Cartwright, J., and James, D. (2006). Frontally Confined versus Frontally Emergent Submarine Landslides: a 3D Seismic Characterisation. *Mar. Pet. Geology.* 23, 585–604. doi:10.1016/j.marpetgeo.2006.04.002

Germa, A., Lahitte, P., and Quidelleur, X. (2015). Construction and Destruction of Mont Pelée Volcano: Volumes and Rates Constrained from a Geomorphological Model of Evolution. *J. Geophys. Res. Earth Surf.* 120 (7), 1206–1226. doi:10.1002/2014jf003355

Germa, A., Quidelleur, X., Labanieh, S., Chauvel, C., and Lahitte, P. (2011b). The Volcanic Evolution of Martinique Island: Insights from K-Ar Dating into the Lesser Antilles Arc Migration since the Oligocene. *J. Volcanology Geothermal Res.* 208, 122–135. doi:10.1016/j.jvolgeores.2011.09.007

Germa, A., Quidelleur, X., Labanieh, S., Lahitte, P., and Chauvel, C. (2010). The Eruptive History of Morne Jacob Volcano (Martinique Island, French West Indies): Geochronology, Geomorphology and Geochemistry of the Earliest Volcanism in the Recent Lesser Antilles Arc. *J. Volcanology Geothermal Res.* 198 (3–4), 297–310. doi:10.1016/j.jvolgeores.2010.09.013

Germa, A., Quidelleur, X., Lahitte, P., Labanieh, S., and Chauvel, C. (2011a). The K-Ar Cassignol-Gillot Technique Applied to Western Martinique Lavas: A Record of Lesser Antilles Arc Activity from 2Ma to Mount Pelée Volcanism. *Quat. Geochronol.* 6, 341–355. doi:10.1016/j.quageo.2011.02.001

Gourgaud, A., Fichaut, M., and Joron, J.-L. (1989). Magmatology of Mt. Pelée (Martinique, F.W.I.), I, Magma Mixing and Triggering of the 1902 and 1292 Pelean Nuées Ardentes. *J. Volcanol. Geotherm. Res.* 38 (1– 2), 143–169. doi:10.1016/0377-0273(89)90035-8

Griggs, A. J., Davies, S. M., Abbott, P. M., Rasmussen, T. L., and Palmer, A. P. (2014). Optimising the Use of marine Tephrochronology in the North Atlantic: a Detailed Investigation of the Faroe Marine Ash Zones II, III and IV. *Quat. Sci. Rev.* 106, 122–139. doi:10.1016/j.quascirev.2014.04.031

Gurenko, A. A., Trumbull, R. B., Thomas, R., and Lindsay, J. M. (2005). A Melt Inclusion Record of Volatiles, Trace Elements and Li-B Isotope Variations in a Single Magma System from the Plat Pays Volcanic Complex, Dominica, Lesser Antilles. *Jour. Petrol.* 46, 2495–2526. doi:10.1093/petrology/egi063

Halama, R., Boudon, G., Villemant, B., Joron, J.-L., Le Friant, A., and Komorowski, J.-C. (2006). Pre-eruptive Crystallization Conditions of Mafic and Silicic Magmas at the Plat Pays Volcanic Complex, Dominica (Lesser Antilles). *J. Volcanology Geothermal Res.* 153, 200–220. doi:10.1016/j.jvolgeores.2005.12.001

Hornbach, M. J., Manga, M., Genecov, M., Valdez, R., Miller, P., Saffer, D., et al. (2015). Permeability and Pressure Measurements in Lesser Antilles Submarine Slides: Evidence for Pressure-driven Slow-slip Failure. *J. Geophys. Res. Solid Earth* 120 (12), 7986–8011. doi:10.1002/2015JB012061

Howe, T. M., Lindsay, J. M., Shane, P., Schmitt, A. K., and Stockli, D. F. (2014). Re-evaluation of the Roseau Tuff Eruptive Sequence and Other Ignimbrites in Dominica, Lesser Antilles. *J. Quat. Sci.* 29, 531–546. doi:10.1002/jqs.2723

Jaupart, C., and Allègre, C. J. (1991). Gas Content, Eruption Rate and Instabilities of Eruption Regime in Silicic Volcanoes. *Earth Planet. Sci. Lett.* 102, 413–429. doi:10.1016/0012-821x(91)90032-d

Jutzeler, M., Manga, M., White, J. D. L., Talling, P. J., Proussevitch, A. A., Watt, S. F. L., et al. (2017). Submarine Deposits from Pumiceous Pyroclastic Density Currents Traveling over Water: An Outstanding Example from Offshore Montserrat (IODP 340). *Geol. Soc. America Bull.* 129 (3_4), 392–414. doi:10.1130/B31448.1

Jutzeler, M., White, J. D. L., Talling, P. J., McCanta, M., Morgan, S., Le Friant, A., et al. (2014). Coring Disturbances in IODP Piston Cores with Implications for Offshore Record of Volcanic Events and the Missoula Megafloods. *Geochem. Geophys. Geosyst.* 15, 3572–3590. doi:10.1002/2014GC005447

Keller, J., Ryan, W. B. F., Ninkovich, D., and Altherr, R. (1978). Explosive Volcanic Activity in the Mediterranean over the Past 200,000 Yr as Recorded in Deep-Sea Sediments. *Geol. Soc. America Bull.* 89, 591–604. doi:10.1130/0016-7606(1978)89<591:evaitm>2.0.co;2

Knappe, E., Manga, M., and Le Friant, A. (2020). Rheology of Natural Sediments and its Influence on the Settling of Dropstones in Hemipelagic Marine Sediment. *Earth Space Sci.* 7 (3), e2019EA000876. doi:10.1029/2019EA000876

Labanieh, S., Chauvel, C., Germa, A., Quidelleur, X., and Lewin, E. (2010). Isotopic Hyperbolas Constrain Sources and Processes under the Lesser Antilles Arc. *Earth Planet. Sci. Lett.* 298, 35–46. doi:10.1016/j.epsl.2010.07.018

Labanieh, S., Chauvel, C., Germa, A., and Quidelleur, X. (2012). Martinique: a clear Case for Sediment Melting and Slab Dehydration as a Function of Distance to the Trench. *Jour. Petrol.* 53 (12), 2441–2464. doi:10.1093/petrology/egs055

Lacroix, A. (1904). *La Montagne Pelée et ses Eruptions*. Paris: Masson, 662.

Lafuerza, S., Le Friant, A., Manga, M., Boudon, G., Villemant, B., Stroncik, N., et al. (2014). "Geomechanical Characterizations of Submarine Volcano Flank Sediments, Martinique, Lesser Antilles Arc, Chap. 7," *Sumarine Mass Movements and Consequences, Advances in Natural and Technological Hazards Research*. S. Krastel, J.-H. Behrmann, D. Völker, M. Stipp, C. Berndt, R. Urgeles, et al. Editors (Cham, Switzerland: Springer International), 73. doi:10.1007/978-3-319-00972-8_7

Le Friant, A., Boudon, G., Deplus, C., and Villemant, B. (2003). Large-scale Flank Collapse Events during the Activity of Montagne Pelée, Martinique, Lesser Antilles. *J. Geophys. Res.* 108 (B1), 2055. doi:10.1029/2001JB001624

Le Friant, A., Boudon, G., Komorowski, J.-C., and Deplus, C. (2002). L'île de la Dominique, à l'origine des avalanches de débris les plus volumineuses de l'arc des Petites Antilles. *Comptes Rendus Geosci.* 334, 235–243. doi:10.1016/s1631-0713(02)01742-x

Le Friant, A., Ishizuka, O., Boudon, G., Palmer, M. R., Talling, P. J., Villemant, B., et al. (2015). Submarine Record of Volcanic Island Construction and Collapse in the Lesser Antilles Arc: First Scientific Drilling of Submarine Volcanic Island Landslides by IODPExpedition 340. *Geochem. Geophys. Geosyst.* 16, 420–442. doi:10.1002/2014GC005652

Le Friant, A., Ishizuka, O., and Stroncik, N. A.; the Expedition 340 Scientists (2013). *Proc. IODP*. Tokyo: Integrated Ocean Drilling Program Management International, Inc., 340. doi:10.2204/iodp.proc.340.109.2013

Le Friant, A., Lebas, E., Brunet, M., Lafuerza, S., Hornbach, M., Coussens, M., et al. and Submarine Landslides Around Volcanic Islands, (2019). Submarine Landslides Around Volcanic Islands: A Review of what Can Be Learned from the Lesser Antilles Arc. AGU Book "*Submarine Landslides: Subaqueous Mass Transport Deposits from Outcrops to Seismic Profiles*" Edited by K. Ogata, A. Festa, and G. A. Pini. (USA: American Geophysical Union, John Wiley & Sons Inc.,), 277-297. doi:10.1002/9781119500513.ch17

Le Friant, A., Lock, E. J., Hart, M. B., Boudon, G., Sparks, R. S. J., Leng, M. J., et al. (2008). Late Pleistocene Tephrochronology of marine Sediments Adjacent to Montserrat, Lesser Antilles Volcanic Arc. *J. Geol. Soc.* 165 (1), 279–289. doi:10.1144/0016-76492007-019

Lebas, E., Le Friant, A., Boudon, G., Watt, S. F. L., Talling, P. J., Feuillet, N., et al. (2011). Multiple Widespread Landslides during the Long-Term Evolution of a Volcanic Island: Insights from High-Resolution Seismic Data, Montserrat, Lesser Antilles. *Geochem. Geophys. Geosystems* 12, Q05006. doi:10.1029/2010gc003451

Lindsay, J. M., Smith, A. L., Roobol, M. J., and Stasiuk, M. V. (2005). "Dominica," in *Volcanic Hazard Atlas of the Lesser Antilles*. Editors J. M. Lindsay, R. E. A. Robertson, J. B. Shepherd, and S. Ali (Trinidad and Tobago, W.I.: Seismic Research Unit. the University of West Indies), 1–48. doi:10.1016/j.jvolgeores.2005.04.018

Lisiecki, L. E., and Raymo, M. E. (2005). A Pliocene-Pleistocene Stack of 57 Globally Distributed Benthic δ18O records18O Records. *Paleoceanography* 20, 1–17. doi:10.1029/2004PA001071

Llopart, J., Lafuerza, S., Le Friant, A., Urgeles, R., and Watremez, L. (2018). "Hydrogeological Evolution as a Pre-conditioning Factor for Slope Failure in a Back-arc Volcanic Setting, W off Martinique Island,". Paper presented at 8th International Symposium on Submarine Mass Movements and their consequences (ISSMMTC), 7–9 May 2018 (Victoria: British Columbia).

Lowe, D. J. (2014). "Marine Tephrochronology: a Personal Perspective," in *Geological Society*. Editors P. M. Abbott, S. M. Davies, N. J. G. Pearce, and S. Wastegard (London: Special Publications), 398, 7–19. doi:10.1144/sp398.11

Lowe, D. J. (2011). Tephrochronology and its Application: a Review. *Quat. Geochronol.* 6, 107–153. doi:10.1016/j.quageo.2010.08.003

Martel, C., Pichavant, M., Bourdier, J., Traineau, H., Holtz, F., and Scaillet, B. (1998). Magma Storage Conditions and Control of Eruption Regime in Silicic Volcanoes: Experimental Evidence from Mt. Pelée. *Earth Planet. Sci. Lett.* 156, 89–99. doi:10.1016/S0012-821X(98)00003-X

Martin-Kaye, P. H. A. (1969). A Summary of the Geology of the Lesser Antilles. *Overseas Geology. Mineral Resour.* 10 (2), 172–206.

Mencaroni, D., Llopart, J., Urgeles, R., Lafuerza, S., Gràcia, E., Le Friant, A., et al. (2020). From Gravity Cores to Overpressure History: the Importance of Measured Sediment Physical Properties in Hydrogeological Models. *Geol. Soc. Lond. Spec. Publications* 500, 289–300. doi:10.1144/SP500-2019-176

Michaud-Dubuy, A., Carazzo, G., Tait, S., Le Hir, G., Fluteau, F., and Kaminski, E. (2019). Impact of Wind Direction Variability on hazard Assessment in Martinique (Lesser Antilles): The Example of the 13.5 Ka Cal BP Bellefontaine Plinian Eruption of Mount Pelée Volcano. *J. Volcanology Geothermal Res.* 381, 193–208. doi:10.1016/j.jvolgeores.2019.06.004

Pamela Reid, R., Carey, S. N., and Ross, D. R. (1996). Late Quaternary Sedimentation in the Lesser Antilles Island Arc. *Geol. Soc. Am. Bull.* 108, 78–100. doi:10.1130/0016-7606(1996)108<0078:lqsitl>2.3.co;2

Paterne, M., Guichard, F., Labeyrie, J., Gillot, P. Y., and Duplessy, J. C. (1986). Tyrrhenian Sea Tephrochronology of the Oxygen Isotope Record for the Past 60,000 Years. *Mar. Geology.* 72 (3-4), 259–285. doi:10.1016/0025-3227(86)90123-4

Pichavant, M., Martel, C., Bourdier, J. L., and Scaillet, B. (2002). Physical Conditions, Structure and Dynamics of a Zoned Magma Chamber: Mount Pelée (Martinique, Lesser Antilles Arc). *J. Geophys. Res.* 107 (B5), 1–25. doi:10.1029/2001jb000315

Quidelleur, X., Hildenbrand, A., and Samper, A. (2008). Causal Link between Quaternary Paleoclimatic Changes and Volcanic Islands Evolution. *Geophys. Res. Lett.* 35, L02303. doi:10.1029/2007GL031849

Reimer, P. J., Bard, E., Bayliss, A., Beck, J. W., Blackwell, P. G., Bronk, H., et al. (2013a). IntCal13 and MARINE13 Radiocarbon Age Calibration Curves 0-50000 Years calBP. *Radiocarbon* 55 (4), 1869–1887. doi:10.2458/azu_js_rc.55.16947

Reimer, P. J., Bard, E., Bayliss, A., Beck, J. W., Blackwell, P. G., Ramsey, C. B., et al. (2013b). Selection and Treatment of Data for Radiocarbon Calibration: an Update to the International Calibration (IntCal) Criteria. *Radiocarbon* 55 (4), 1923–1945. doi:10.2458/azu_js_rc.55.16955

Roobol, M. J., and Smith, A. L. (1976). Mount Pelée, Martinique: A Pattern of Alternating Eruptive Styles. *Geology* 4, 521–524. doi:10.1130/0091-7613(1976)4<521:mpmapo>2.0.co;2

Samper, A., Quidelleur, X., Boudon, G., Le Friant, A., and Komorowski, J. C. (2008). Radiometric Dating of Three Large Volume Flank Collapses in the Lesser Antilles Arc. *J. Volcanology Geothermal Res.* 176, 485–492. doi:10.1016/j.jvolgeores.2008.04.018

Sigurdsson, H., Sparks, R. S. J., Carey, S. N., and Huang, T. C. (1980). Volcanogenic Sedimentation in the Lesser Antilles Arc. *J. Geology.* 88, 523–540. doi:10.1086/628542

Solaro, C., Boudon, G., Le Friant, A., Balcone-Boissard, H., Emmanuel, L., and Paterne, M. (2020). New Insights into the Recent Eruptive History and Collapse History of Montagne Pelée (Lesser Antilles Arc) from Offshore marine Drilling Site U1401A (340 Expedition IODP). *J. Volcanology Geothermal Res.* 403, 107001. doi:10.1016/j.jvolgeores.2020.107001

Sparks, R. S. J., Sigurdsson, H., and Carey, S. N. (1980a). The Entrance of Pyroclastic Flows into the Sea I. Oceanographic and Geologic Evidence from dominica, Lesser Antilles. *J. Volcanology Geothermal Res.* 7, 87–96. doi:10.1016/0377-0273(80)90021-9

Sparks, R. S. J., Sigurdsson, H., and Carey, S. N. (1980b). The Entrance of Pyroclastic Flows into the Sea, II. Theoretical Considerations on Subaqueous Emplacement and Welding. *J. Volcanology Geothermal Res.* 7, 97–105. doi:10.1016/0377-0273(80)90022-0

Stuiver, M., and Reimer, P. J. (1993). Extended 14C Data Base and Revised CALIB 3.0 14C Age Calibration Program. *Radiocarbon* 35, 215–230. doi:10.1017/s0033822200013904

Talling, P. J. (2013). Hybrid Submarine Flows Comprising Turbidity Current and Cohesive Debris Flow: Deposits, Theoretical and Experimental Analyses, and Generalized Models. *Geosphere* 9, 460–488. doi:10.1130/ges00793.1

Talling, P. J., Masson, D. G., Sumner, E. J., and Malgesini, G. (2012). Subaqueous Sediment Density Flows: Depositional Processes and deposit Types. *Sedimentology* 59, 1937–2003. doi:10.1111/j.1365-3091.2012.01353.x

Talling, P. J. (2014). On the Triggers, Resulting Flow Types and Frequencies of Subaqueous Sediment Density Flows in Different Settings. *Mar. Geology.* 352, 155–182. doi:10.1016/j.margeo.2014.02.006

Talling, P. J., Wynn, R. B., Schmmidt, D. N., Rixon, R., Sumner, E., and Amy, L. (2010). How Did Thin Submarine Debris Flows Carry Boulder-Sized Intraclasts for Remarkable Distances across Low Gradients to the Far Reaches of the Mississippi Fan? *J. Sediment. Res.* 80, 829–851. doi:10.2110/jsr.2010.076

Tanguy, J.-C. (2004). Rapid Dome Growth at Montagne Pelée during the Early Stages of the 1902?1905 Eruption: a Reconstruction from Lacroix?s Data. *Bull. Volcanol* 66, 615–621. doi:10.1007/s00445-004-0344-z

Tanguy, J.-C. (1994). The 1902-1905 Eruptions of Montagne Pelée, Martinique: Anatomy and Retrospection. *J. Volcanology Geothermal Res.* 60, 87–107. doi:10.1016/0377-0273(94)90064-7

Traineau, H., Westercamp, D., Bardintzeff, J. M., and Miskovski, J. C. (1989). The recent pumice eruptions of Mt. Pele´e volcano, Martinique, part I, Depositional sequences, description of pumiceous deposits. *J. Volcanol. Geotherm. Res.* 38 (1– 2), 17–33. doi:10.1016/0377-0273(89)90027-9

Trofimovs, J., Fisher, J. K., Macdonald, H. A., Talling, P. J., Sparks, R. S. J., Hart, M. B., et al. (2010). Evidence for Carbonate Platform Failure during Rapid Sea-Level Rise; Ca 14 000 Year Old Bioclastic Flow Deposits in the Lesser Antilles. *Sedimentology* 57, 735–759. doi:10.1111/j.1365-3091.2009.01117.x

Trofimovs, J., Talling, P. J., Fisher, J. K., Sparks, R. S. J., Watt, S. F. L., Hart, M. B., et al. (2013). Timing, Origin and Emplacement Dynamics of Mass Flows Offshore of SE Montserrat in the Last 110 Ka: Implications for Landslide and Tsunami Hazards, Eruption History, and Volcanic Island Evolution. *Geochem. Geophys. Geosyst.* 14, 385–406. doi:10.1002/ggge.20052

Villemant, B., Boudon, G., and Komorowski, J.-C. (1996). U-series Disequilibrium in Arc Magmas Induced by Water-Magma Interaction. *Earth Planet. Sci. Lett.* 140, 259–267. doi:10.1016/0012-821x(96)00035-0

Villemant, B., and Boudon, G. (1998). Transition from Dome-Forming to Plinian Eruptive Styles Controlled by H2O and Cl Degassing. *Nature* 392, 65–69. doi:10.1038/32144

Vincent, P. M., Bourdier, J. L., and Boudon, G. (1989). The Primitive Volcano of Mount Pelée: Its Construction and Partial Destruction by £Ank Collapse. *J. Volcanol. Geotherm. Res.* 38, 1–15.

Wadge, G. (1984). Comparison of Volcanic Production Rates and Subduction Rates in the Lesser Antilles and Central America. *Geol* 12, 555–558. doi:10.1130/0091-7613(1984)12<555:covpra>2.0.co;2

Wall-Palmer, D., Coussens, M., Talling, P. J., Jutzeler, M., Cassidy, M., Marchant, I., et al. (2014). Late Pleistocene Stratigraphy of IODP Site U1396 and Compiled Chronology Offshore of South and South West Montserrat, Lesser Antilles. *Geochem. Geophys. Geosyst.* 15, 3000–3020. doi:10.1002/2014GC005402

Watt, S. F. L., Talling, P. J., Vardy, M. E., Masson, D. G., Henstock, T. J., Hühnerbach, V., et al. (2012). Widespread and Progressive Seafloor-Sediment Failure Following Volcanic Debris Avalanche Emplacement: Landslide Dynamics and Timing Offshore Montserrat, Lesser Antilles. *Mar. Geology.* 323-325, 69–94. doi:10.1016/j.margeo.2012.08.002

Watt, S. F. L. (2019). The Evolution of Volcanic Systems Following Sector Collapse. *J. Volcanology Geothermal Res.* 384, 280–303. doi:10.1016/j.jvolgeores.2019.05.012

Westercamp, D., Andreieff, P., Bouysse, P., Cottez, S., and Battistini, R. (1989). "Martinique," in *Carte géologique à 1/50 000* (Orleans: BRGM).

Westercamp, D., and Traineau, H. (1983b). *Carte géologique au 1/20 000 de la Montagne Pelée, avec notice explicative*. Orleans: BRGM.

Westercamp, D., and Traineau, H. (1983a). The Past 5,000 Years of Volcanic Activity at Mt. Pelee Martinique (F.W.I.): Implications for Assessment of Volcanic Hazards. *J. Volcanology Geothermal Res.* 17, 159–185. doi:10.1016/0377-0273(83)90066-5

Whitham, A. G. (1989). The Behaviour of Subaerially Produced Pyroclastic Flows in a Subaqueous Environment: Evidence from the Roseau Eruption, Dominica, West Indies. *Mar. Geology.* 86, 27–40. doi:10.1016/0025-3227(89)90016-9

Conflict of Interest: The authors declare that the research was conducted in the absence of any commercial or financial relationships that could be construed as a potential conflict of interest.

Publisher's Note: All claims expressed in this article are solely those of the authors and do not necessarily represent those of their affiliated organizations, or those of the publisher, the editors and the reviewers. Any product that may be evaluated in this article, or claim that may be made by its manufacturer, is not guaranteed or endorsed by the publisher.

Copyright © 2022 Villemant, Le Friant, Caron, Del Manzo, Lafuerza, Emmanuel, Ishizuka, Guyard, Labourdette, Michel and Hidalgo. This is an open-access article distributed under the terms of the Creative Commons Attribution License (CC BY). The use, distribution or reproduction in other forums is permitted, provided the original author(s) and the copyright owner(s) are credited and that the original publication in this journal is cited, in accordance with accepted academic practice. No use, distribution or reproduction is permitted which does not comply with these terms.